First publ. in: International Journal of Mass Spectrometry and Ion Processes 159 (1996), 1-3, pp. 81-109

CO chemisorption on Ni_n, Pd_n and Pt_n clusters

G. Ganteför*, G. Schulze Icking-Konert, H. Handschuh, W. Eberhardt

Institut für Festkörperforschung, Forschungszentrum Jülich, 52425, Jülich, Germany

Abstract

Vibrationally resolved photoelectron spectra of mass-selected negatively charged Ni_n^- ($n = 1-3$), Pd_n^- ($n = 2, 3$) and Pt_n^- ($n = 1-4$) clusters are compared with the corresponding spectra of these clusters ligated with m CO molecules ($m = 1-8$). The spectra of the $Pt_n(CO)_m^-$ species reveal part of the valence orbitals, which actually form the chemisorption bond. The data are in good agreement with the Blyholder model for CO chemisorption (σ-donation–π-backdonation scheme) and indicate that saturation corresponds to the formation of a closed electronic shell of the neutral. The strength of the π-backdonation is found to be larger for small particles compared with the corresponding single crystal surfaces, which may be related to the catalytic properties of small particles. The spectra of the unsaturated $Ni_n(CO)_m^-$ show fundamental differences compared with the ones of $Pt_n(CO)_m^-$ clusters owing to the high degree of localization of the Ni 3d orbitals. The spectra of the $Pd_n(CO)_m^-$ species show a rather irregular behaviour.

Keywords: Carbon monoxide; Cluster; Chemisorption

PACS classification: 36.40. + d; 73.20.Hb; 82.65.My

1. Introduction

In the past two decades the study of the bond of a CO molecule to a metal surface has attracted considerable attention [1–5]. The wealth of experimental information, especially the studies of the electronic structure using photoelectron spectroscopy [3–9] as well as frequency shifts observed in vibrational spectroscopy [10–16], have been interpreted using different theoretical approaches [17–36]. The standard model for the electronic interactions between CO and a surface has been formulated by Blyholder [2]. As early as 1960–1970 the electronic structure of metal carbonyls has been analysed using similar techniques (photoelectron spectroscopy [37–39], vibrational spectroscopy [40–49]) inspiring the development of theoretical models [50–64] of the chemical bond in such a compound. For both areas of research the understanding of the basic interaction of a single CO with an isolated metal atom is of fundamental interest and there is a considerable amount of theoretical effort [65–74] focused on the most simple molecular configurations of the type M–CO with M = Ni, Pd, Pt. To our knowledge, from these studies no fundamental difference between the CO bonding to a surface and to a small metal particle has been unambiguously identified. However, since small particles have special catalytic properties, such differences should exist.

* Corresponding author.

Metal clusters ligated with CO are expected to bridge the gap between the surface and the carbonyl [75,76]. With increasing size the properties of the bare clusters change from a molecular to bulk behaviour. In cluster experiments the coverage of CO on the cluster can be varied continuously from the bare cluster up to the saturated species, the metal carbonyl [77–81]. So far, experimental studies of these species focused on the determination of the reaction rates and the maximum uptake of CO on a certain cluster, i.e., the saturation limits. The saturation limits are explained using Lauhers valence electron counting rules [62–64,81]. These rules base on the concept that the saturated carbonyl achieves a closed shell electronic structure for a certain "magic" number of valence electrons (e.g. 18 for $Ni_1(CO)_4$). Each CO donates 2 electrons to the cluster and the Ni atom has 10 valence electrons. According to this approach, the number of ligands depends on the number of valence electrons of the metal atoms and, as a small correction, on the geometry of the metal core. The geometry of the metal core determines the number of antibonding metal orbitals not available for electrons. Thus, in cases of small metal cores and stable carbonyls their experimentally determined structures can be rationalized by the counting rule model.

One inconsistency of this model arises from the fact, that the observed saturation limits depend on the transition metal, even if the metals have the same number of valence electrons (e.g. Ni and Pt [81]). The approach of the electron counting rules also does not include a significant contribution from steric hindrance between the CO molecules, which governs the saturation on a metal surface. For N_2, which is isoelectronic to CO, a model based on geometric effects only has been used for the explanation of the saturation limits on Ni clusters [82]. It is assumed, that one N_2 binds to one Ni atom at the surface of the cluster on an "on-top" site. The number of adsorbed molecules equals the number of surface metal atoms and thus also contains information about the geometric structure of the metal cluster. In a recent experiment, large differences between the uptake of N_2 for Ni_n^-, Pd_n^- and Pt_n^- clusters clearly demonstrate the danger of these oversimplified chemisorption models [83].

The Blyholder model [1,2,76] gives a more detailed picture of the interaction of the orbitals of CO and the metal surface atoms forming the chemisorption bond. This approach involves highly localized interactions between the CO molecule and the metal atoms only and, therefore, does not give an explanation for the saturation of carbonyls (electronic saturation according to the counting rules) or on surfaces (geometric saturation caused by the repulsive interactions between neighbouring COs).

We here examine the electronic structure of ligated transition metal cluster anions $M_n(CO)_m^-$ (M = Ni, Pd and Pt) using vibrationally resolved photoelectron spectroscopy of negatively charged particles [84–89]. The photoelectron spectra contain information about both the electronic and the geometric structure of the bare and ligated clusters and give some further insight into the interactions responsible for the reactivities and saturation limits determined in cluster chemical reaction rate measurements. The vibrational data can be directly compared with the corresponding data of neutral carbonyls [40–49] and surfaces [10–16], because in photoelectron spectroscopy the final state is examined, which is the neutral one in case of negatively charged species. Since in the clusters an additional electron is present our results can also be compared with inverse photoemission data [6–9]. We address the following questions in our experiment:

1. What kind of interactions form the chemisorption bond?
2. What is the cause for saturation and what determines the limits?
3. What are the differences between CO chemisorption to a metal surface and a metal cluster?

We are able to explain most of the differences and similarities of the $Ni_n(CO)_m^-$, $Pd_n(CO)_m^-$ and

$Pt_n(CO)_m^-$ clusters using the Blyholder model developed for CO chemisorption on surfaces [1,2,76]. In our experiment we study the orbitals close to the HOMO (highest occupied molecular orbital) revealing the chemisorption induced changes of the valence orbitals. The data support the prediction (see, e.g. [53,57,76]) of a destabilization of the metal s orbitals corresponding to a change in the configuration from d^9s in the bare cluster to d^{10} in the saturated species. The spectra of the unsaturated $Pt_n(CO)_m^-$ clusters show a pattern typical for open-shell species, while the ones of the saturated species indicate the formation of a closed electronic shell, which is therefore interpreted to be the reason for saturation. The photoelectron spectra of $Ni_n(CO)_m^-$ reveal significant differences of the electronic structure compared with the $Pt_n(CO)_m^-$ species which can only be explained introducing correlation effects. The correlation effects are related to the ferromagnetic properties of Ni clusters [53,76]. We find a CO stretch vibration frequency for a single CO bound to a Ni_2 and a Ni_3 cluster, which is lower than any such frequency measured for a Ni surface. This might indicate an enhanced π-backdonation interaction in small clusters with respect to the corresponding surface.

It is well known, that in contrast to Ni and Pt there are no "stable" Pd carbonyls [49]. In the literature we could find no straightforward explanation for this property of Pd. On the other hand, the bonding of CO to Pd surfaces does not differ much from the one to Ni and Pt surfaces [34]. Our photoelectron spectra of the $Pd_n(CO)_m^-$ cluster anions reveal large differences to the ones of Ni and Pt species, which might be related to the preference of a d^{10} configuration of the Pd atoms in small clusters [27].

In Section 2 we briefly review the huge amount of experimental and theoretical results in areas related to our experiment. In Section 3 we describe the experiment and in Section 4 we discuss the results. The conclusion in Section 5 puts our findings in perspective with the previous results described in Section 2.

2. Review

2.1. Experimental data of CO adsorbed on Ni, Pd and Pt surfaces

2.1.1. Photoelectron spectroscopy

With UV photoelectron spectroscopy the valence band structure of metal surfaces covered with CO can be analysed [3–5]. However, the energy region close to the Fermi energy is dominated by emission from the metal d bands. Because of the high density of states and the congestion of bands an analysis of the changes induced by adsorption is difficult. At higher binding energies emission from the 4σ, 1π and 5σ orbitals of CO is observed. While in gaseous CO the 1π and 5σ levels are well separated by about 3 eV, in CO adsorbed on many transition metals the 5σ orbital is stabilized by the chemisorption (Blyholder model [1,2]) and almost degenerate with the 1π orbital (at about 7–9 eV below the Fermi energy E_F). This indicates, that the 5σ orbital strongly interacts with the metal, while the other two occupied levels of CO (4σ, 1π) play only a minor rule in the formation of the bond. The unoccupied CO 2π orbital, which is also strongly involved into the chemisorption, has been studied by inverse photoemission [6–9].

2.1.2. Vibrational spectroscopy

In most cases the CO molecule is vertically adsorbed with the carbon atom oriented towards the surface [1]. The molecule can absorb on different sites on a single crystal surface [2,10]. The most common ones are an "on-top" site with the CO molecule bound to a single metal atom, a "bridge" site in between two neighbouring metal atoms in a row and a "hollow" site in between three neighbouring metal atoms forming a triangle on the surface. In a free CO molecule the stretch vibration has an energy of 2143 cm^{-1} [90]. This energy decreases owing to adsorption depending on the site [10–16]. In most transition metals the on-top site frequency is about 2050 cm^{-1}, the bridge site frequency is about

Table 1
Vibration frequencies of CO adsorbed on surfaces

	On top	Bridge[a]	Hollow[a]	Ref.
Ni 111	2045 (0.57)	1900 (0.33)	1817 (< 0.1)	[10]
Ni 100	2069 (0.5)	1932 (0.3)		[14]
Ni 111	2049	1830	1818	[42]
Pd 100	2096	1895		[10]
Pd 111	2095 (0.75)	1948 (0.5)	1813 (0)	[10]
Pd 210		1878		[10]
Pd 111	2092	1865	1820	[42]
Pt 111	2065 (< 0.1)	1870 (0.5)		[10]
Pt 111	2104 (0.5)	1855 (0.5)		[12]
Pt 111	2100 (0.17)	1850 (0.24)		[13]
Pt 111	2068 (< 0.1)	1840 (0.5)	1810 (0.4)[b]	[16]
Pt 111	2084	1850	1820[b]	[42]

The energies of the stretch vibrational mode of CO molecules adsorbed at different sites on Ni, Pd and Pt surfaces. The frequency depends on the coverage and the coverage is given in some cases in parenthesis. The energy of the stretch vibration mode of free CO molecules is 2143 cm^{-1} [90]. All values are given in wavenumbers (cm^{-1}).

[a] In terms of the assignment of an adsorption geometry (bridge or hollow) we list the assignments given by the respective references. We are well aware of the fact that some of these assignments have been contradicted by other recent experiments [92].

[b] The low frequency assigned to a hollow site on Pt(111) has not been reproduced in a more recent experiment [91].

1900 cm^{-1} and the hollow site one about 1800 cm^{-1} with a variation of about $\pm$ 50 cm^{-1} depending on the metal [42]. Table 1 shows some representative data of Ni, Pd and Pt surfaces. The assignment of certain observed frequencies to certain binding sites is not always unambiguous. For example, the low frequency (Table 1: 1810 cm^{-1}) assigned to a hollow site on Pt(111) has not been reproduced in a more recent measurement [91].

The vibrational frequency depends on the coverage and is lowest at low coverage. The increase with increasing CO coverage is explained by a smaller "backdonation" [45] and the CO–CO dipole interaction [15]. Therefore, for a comparison with cluster calculations and carbonyls the frequencies in the limit of zero coverage should be used (if available).

From vibrational spectroscopy [10–16] in comparison with other techniques the site preferences can be determined. On a Pt(111) surface at low coverage CO prefers the on-top site [10,12,13,16,30,34]. At slightly higher coverage also molecules bound in bridge sites are found. On Ni(111) [10,14,34] and Pd(111) [10,28,34] at low coverages CO prefers bridge or hollow sites. However, the binding energies are roughly similar for the three metals and for the different sites and in the range between 1.3–1.6 eV [19,21,28,31,33,34].

Very recently, the adsorbate site of CO on Ni has been determined independently using photoelectron diffraction [92]. These results disagree with the traditional correlation of the range of vibrational frequencies with on-top, bridge and hollow sites given above. Therefore, it seems to be no longer valid to assign a CO adsorbate to a certain site based on the frequency measurement alone. Accordingly, we will refrain from a detailed discussion of adsorption sites except in cases, when the geometry of the carbonyl is known. Than the measured vibrational frequencies might be correlated with certain adsorption sites.

2.1.3. Inverse photoemission

With inverse photoemission [6–9] the unoccupied bands above the Fermi level are detected. For a clean metal surface this are the metal d and s/p bands and surface states. Owing to CO adsorption several features assigned to CO 2π derived bands are found. For free CO the

unoccupied 2π orbital is located 1.6 eV above the vacuum level [7]. Adsorbed on surfaces the CO 2π orbitals form several bands, which hybridise partly with occupied metal d and unoccupied metal s/p bands [9]. According to the inverse photoemission studies, the lowest 2π emission on, e.g. Ni(110) is found to be only 1.5 eV above the Fermi level [9]. This surprisingly high binding energy of the most stable 2π band can be explained by two effects: (i) the hybridization with unoccupied metal d and p bands and (ii) the weakening of the CO bond due to chemisorption resulting in a stabilization of all antibonding CO orbitals.

2.2. Theoretical models of CO chemisorption on surfaces

2.2.1. Blyholder model

Chemisorption on surfaces has been modelled using cluster models [17–32], slab calculations [33–36], carbonyls [50–61] and, most simple, a molecule consisting of a single metal atom and a CO molecule [65–74]. A review of the various approaches has been recently given by Hoffmann [1]. However, it is important to keep in mind the approximations involved in using a simplified model. For example, even the use of molecular orbitals is already a crude approximation, because an independence of the electrons moving in the single particle orbitals is assumed. Another approximation is the assignment of molecular orbitals to be, e.g. CO 2π- or metal d-derived. The molecular orbitals of the compound have contributions from a multitude of occupied and unoccupied states of the separated atoms and the assignment to a dominant character could be misleading.

In the Blyholder model [1,2,53,76] the chemisorption bond is separated into the interaction of the occupied 5σ orbitals of CO with the metal σ valence orbitals (σ-donation) and the one of the unoccupied CO 2π orbitals with the metal d_π orbitals (π-backdonation). In contrast to the treatment of carbonyl complexes (see below) the interaction of a single CO molecule is considered as a localized interaction between a single CO molecule and its next metal atom neighbours (e.g. only one in a on-top site). The metal σ orbitals are predominantly the s/p and d_{z^2} orbitals (the z-axis is chosen parallel to the CO molecular axis). Since the CO 5σ orbital is located at a relatively high BE, it is stabilized by this interaction explaining the shift of the 5σ features in the photoemission spectra (see above). The corresponding metal orbitals (s/p and d_{z^2}) are destabilized and might be even shifted above E_F. This interaction results in a delocalization of the CO 5σ orbital towards the metal corresponding to a charge donation. The other part of the interaction consists of a destabilization of the CO 2π orbital and the metal d_π orbitals are shifted towards higher binding energy. The metal d_π orbitals delocalize into the direction of the CO molecule corresponding to a charge backdonation. This delocalization corresponds to the mixing with the CO 2π orbital. Since the d_π hybrid orbitals are occupied, there is a formal charge in the CO 2π orbital. The 2π orbital is antibonding with respect to the C–O bond and, therefore, chemisorption weakens the CO bond. This explains the observed decrease of the vibrational frequency of the CO stretch mode. In a bridge or hollow site the overlap of the π orbitals is larger resulting in a further decrease of the vibrational frequency (Table 1). The shift of the CO 2π orbital towards lower BE (higher energy above E_F) might be overcompensated by the stabilization of this antibonding orbital corresponding to the weakening of the CO bond [1].

In detail, the CO chemisorption can be separated into three interactions [17,57,66]: (i) CO 5σ–metal s/p, (ii) CO 5σ–metal d_{z^2} and (iii) CO 2π–metal d_π. Interactions (i) and (ii) correspond to charge donation and (iii) to backdonation. The resulting hybrid orbitals can still be characterized by their predominant component and assume the following ordering of the binding energies in case of saturation: CO 5σ > metal d_π > metal d_{z^2} > CO 2π > metal s/p. If the metal atoms have

10 or more valence electrons, all metal d orbitals are occupied. Accordingly, the CO 5σ–metal d_{z^2} interaction is non-bonding, because the bonding (= CO 5σ) and antibonding (= metal d_{z^2}) orbitals are occupied [57,66]. For transition metals with a smaller number of valence electrons (e.g. Fe = 8 electrons) the metal d_{z^2} orbitals are unoccupied and the CO 5σ–metal d_{z^2} interaction is bonding.

2.2.2. The bonding in Ni(CO), Pd(CO) and Pt(CO)

The smallest aggregates with a metal–CO bond are molecules like NiCO, which can be treated theoretically on a high level [65–74]. The $^1\Sigma^+$ electronic ground state of NiCO [65–67,70,74] corresponds to a bond between the CO in its $^1\Sigma^+$ ground state to a Ni atom in the ^{1}S excited state corresponding to a d^{10} configuration. Although this is an excited state of the Ni atom, the total energy of the compound is lower than for a NiCO system, where the Ni atom is in the d^9s configuration. This is due to the repulsive interaction between the CO 5σ orbital and the occupied metal 4s orbital. These calculations support the simplified model of chemisorption (Figs 1 and 2, see later) and the separation of CO chemisorption into three components (CO

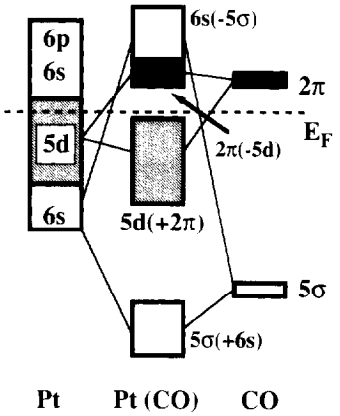

Fig. 1. Simplified scheme of the interactions responsible for the formation of the chemisorption bond of CO to Pt according to the Blyholder model (from Pacchioni et al. [53,76]). Only the interactions of the CO 2π with the Pt 5d and the CO 5σ with the Pt 6s orbitals are considered.

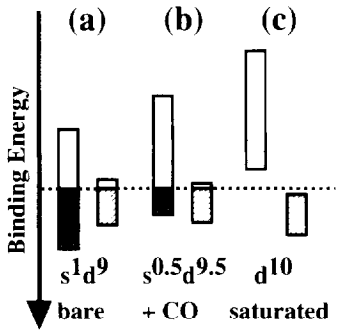

Fig. 2. Schematic picture of the valence orbitals of a bare (a), a partially ligated (b) and a saturated (c) transition metal cluster. The long bar indicates the s/p-derived orbitals, the short bar the d-derived orbitals. The dotted line is the boarder between the occupied and unoccupied orbitals. The CO derived orbitals (2π at low binding energy and 5σ at higher binding energy) are not included. In the ligated cluster the metal s/p and d (hybrid) orbitals have a certain admixture from CO 5σ and 2π orbitals, respectively, which is also neglected for simplification.

5σ–metal s/p; CO 5σ–metal d_{z^2}; CO 2π–metal d_π). Bauschlicher et al. [66] found the π-back-donation to be the largest contribution to the bonding and dependent on the occupation number in the d_{z^2} orbital (2 for Cu; 1 for Ni; 0 for Fe) the σ-donation contributes up to 40% to the binding energy (FeCO).

According to similar calculations for $NiCO^-$ [68] the additional electron occupies an orbital with a predominant metal s/p character, which is the one that is destabilized by the repulsive interaction with the CO 5σ orbitals. These calculations on the anion resulted in an assignment of the features observed in the photoelectron spectrum of $NiCO^-$ [87].

For PdCO [69–72] and PtCO [69,70,73] the calculations give similar results concerning the ground state ($^1\Sigma^+$) and bonding mechanism as for NiCO. There is some discussion on the relative strength of the chemisorption bond, whether PdCO or NiCO have a higher binding energy. The energy necessary to promote the metal atom into the d^{10} configuration ($\approx$ 1.7 eV for Ni, 0 eV for Pd, $\approx$ 0.7 eV for Pt [93]) is 0 eV for Pd facilitating the formation of the chemisorption bond. However, the high stability of

the d^{10} configuration of Pd results in a weaker interaction, because the closed shell configuration has a lower polarizability. Both the ability to accept and to donate charge are reduced [27,70].

2.2.3. Cluster models

The surface of a metal has been frequently modelled by a cluster with an appropriate geometry [17–32]. In contrast to calculations of carbonyls and real clusters the geometry of these particles is one of a fragment of the bulk. It is assumed, that the interaction of a single CO molecule involves only the atoms close to the adsorption site. The smaller the cluster the easier the calculations. However, with increasing cluster size the calculated properties like the binding energy, the bond distance, the site preferences and the vibrational frequencies exhibit a better agreement with the experimental surface data [22,24,32]. The results of the "surface" clusters cannot be directly compared with data of "real" clusters owing to the difference in geometry. We searched this field to find hints for a systematic difference between the chemisorption of CO to a surface and a small particle caused by finite size effects. However, any deviation between the cluster calculations and the experimental surface data might be due to finite size effects *or* due to the approximations used in the calculations. In the literature we could not find a systematic deviation from surface data caused by the finite size of the particle.

One important finite size effect has been found in a comparison between $Pd_2(CO)$ with $Pd_8(CO)$ with the CO adsorbed in a bridge site [27]. The calculated binding energy increases from 0.79 eV for $Pd_2(CO)$ to 1.72 eV for $Pd_8(CO)$. This increase is attributed to a change in the configuration of the Pd atoms from almost purely d^{10} in the dimer towards the bulk configuration $d^{8.7}$ [94]. Occupied metal s/p orbitals result in a decrease of the CO binding energy due to the σ repulsion. On the other hand, the vacancy formation in the d states results in larger polarizability of the metal d orbitals and an increase of hybridization and thus increasing binding energy. According to the calculation the latter effect is stronger and the binding energy of a CO to a Pd_n cluster increases with n. This is in agreement with the known instability of Pd carbonyls and, on the other hand, with the similarity of the binding energies of CO bound to Ni, Pd and Pt surfaces.

The most important contribution from cluster calculations is the qualitative analysis of the bonding mechanism itself. The Blyholder model has also been supported by slab calculations [1,33–36], which give a detailed analysis of the interactions of the atomic orbitals involved. In this type of calculation the interaction of a 2-dimensional array of CO molecules and a corresponding one of metal atoms (usually 4–5 monolayers) is studied.

2.3. Experimental data of carbonyls

In the present paper we consider carbonyls to be unsupported metal carbonyl complexes in the gas phase. The data can be compared with such on complexes in solution, on condensed-phase carbonyl compounds and on CO molecules chemisorbed on a surface. In any such cases we will notify whether we refer to condensed-phase, liquid solution or surface data. Otherwise, the term carbonyl is used for gas phase species. On-top, bridged and hollow sites correspond to terminal, edge-bridging and face-bridging bonding sites, respectively, using the language of inorganic chemistry.

2.3.1. Photoelectron spectroscopy

The photoelectron spectra of condensed-phase carbonyls [38,39] are very similar to the ones of gas phase carbonyls [37], which is characteristic for stable closed shell molecules. The spectral features can be assigned to emission from the CO 4σ, 1π and 5σ orbitals and at lower BEs from the metal d-derived orbitals [37,38]. The latter ones are different for gas phase carbonyls and for CO adsorbed on metal surfaces. The

spectra of the gas phase carbonyls exhibit only a few narrow peaks, while the data of CO chemisorbed on a surface show an emission signal covering a wider range. This reflects the narrow bandwidth of the metal-derived valence orbitals in a gas phase carbonyl with only a few metal atoms compared with a metal surface with the fully developed band structure. Owing to the limited energy resolution in these experiments it is not possible to reveal the details of the electronic structure, especially the chemisorption induced change in the metal density of states. No vibrational fine structure is resolved.

2.3.2. Vibrational spectroscopy

In $Ni(CO)_4$ there are two frequencies assigned to the C–O stretch mode [40,42,44], the symmetric (2134 cm^{-1}) and the antisymmetric mode (2052 cm^{-1}). In photoelectron spectroscopy only the symmetric stretch mode is observed [87]. The frequencies are determined by different methods like matrix spectroscopy of neutral species [41] or IR spectroscopy of the carbonyl anions in solution [46–48]. Depending on the method there are shifts of the frequency, which depend on the carbonyl and the mode. A few selected frequencies are listed in Table 2. All values of the species with a single metal atom are close to the stretch frequencies of CO molecules bound on-top on a surface (Table 1). As in the case of the surface, the frequency depends on the number of COs in the carbonyl. Timney [43] has proposed a simple method for predicting the CO stretch vibration in saturated mononuclear transition metal carbonyl compounds containing CO and other ligands. Each ligand causes a certain incremental increase in the stretch vibration of a CO molecule bond to the metal atom. The increase is strongest, if the ligand is in trans position, i.e. on the other side of the atom. If the interaction is considered as a competition [45] for charge in the backdonation bond, the strong influence of the trans-ligand can easily be explained, because it is bound to the same d orbital. An increase of the frequency with an increasing number of ligands is also observed for unsaturated carbonyls like the series $Ni(CO)_2$–$Ni(CO)_4$ (Table 2). However, for $Pd(CO)_m$ and $Pt(CO)_m$ the stretch frequency is almost independent of m [44].

For the saturated carbonyls it has been generally accepted, that the observed frequencies are similar to the ones of CO bound in corresponding sites on a surface. De la Cruz et al. [42] estimated from a comparison of a multitude of different carbonyl complexes the average CO stretch frequency in a saturated complex to be 2070 cm^{-1} in

Table 2
Vibration frequencies of carbonyls

Carbonyl	Symmetric	Antisymmetric	Method	Ref.
Saturated carbonyls				
$Ni(CO)_4$	2134	2052	matrix	[41]
$Ni(CO)_4$	2132	2057	gas phase	[40]
$Ni(CO)_4$	2130	2043	matrix	[40]
$Pd(CO)_4$	2122	2066	matrix	[40]
$Pt(CO)_4$	2119	2049	matrix	[40]
Unsaturated carbonyls				
$Ni(CO)_3$	2120	2016	matrix	[41]
$Ni(CO)_2$	2090	1967	matrix	[41]
$Ni(CO)_1$		1996	matrix	[41]
$Pd(CO)_1$		2050	matrix	[71]
$Pd(CO)_2$		2040	matrix	[71]
$Pt(CO)_1$		2052	matrix	[74]

Experimentally determined frequencies of the CO stretch vibration for some selected carbonyls. All values are given in wavenumbers (cm^{-1}).

an on-top site, 1870 cm^{-1} in a bridge site and 1800 cm^{-1} in a hollow site. The values are similar to the ones on the corresponding surfaces (Table 1). On the other hand, the frequency of, e.g. Ni(CO) is lower than the corresponding on-top surface value. From a comparison of the on-top site frequencies of CO adsorbed to Ni, Pd and Pt surfaces with the values of the $M_1(CO)_1$ molecules Kündig et al. [44] concluded, that both σ-donation and π-backdonation must be larger in an (unsaturated) complex compared with the surface.

Many of the stable complexes with more than one metal atom are prepared as anions in solution [46–48]. The vibrational frequencies are determined by IR spectroscopy. To compare these spectra with gas phase or surface data, the frequencies have to be corrected for charge and solvent induced shifts. Calabrese et al. [46,47] prepared a series of dianions $(Pt_3(CO)_6)_n^{2-}$ with $n = 1-10$. $Pt_3(CO)_6^{2-}$ is planar with a triangular Pt_3 core and 3 COs in on-top and 3 in bridge sites. In a similar experiment a corresponding Ni compound $(Ni_3(CO)_6)_2^{2-}$ has been detected [48]. The on-top and bridge frequencies are similar for $(Ni_3(CO)_6)_2^{2-}$ and $(Pt_3(CO)_6)_2^{2-}$.

In the series $(Pt_3(CO)_6)_n^{2-}$ the frequencies decrease with increasing n owing to a larger delocalization of the negative charge. From this dependence the limit for large n might give a rough estimate of the frequencies of neutral $Pt_3(CO)_6$: 2075 cm^{-1} (on-top) and 1895 cm^{-1} (bridge). These values agree roughly with the corresponding surface data (Table 1: 2080 cm^{-1} and 1850 cm^{-1}, respectively). However, the bridge frequency in the carbonyl is higher than even for high coverage data at surfaces. Indeed, the coverage on $Pt_3(CO)_6$ is twice the one of a monolayer (= 2 COs per Pt atom). Since the frequencies increase with increasing CO coverage, this might explain the relatively high bridge frequency in $Pt_3(CO)_6$. This demonstrates, that unambiguous information about differences between the bonding to a surface and to a metal cluster can only be obtained if the frequencies of the neutral $M_n(CO)_1$ species are compared with surface data taken at lowest coverage.

Table 3
CO binding energies in carbonyls

Process	Energy	Ref.
$Ni(CO)_1^- \rightarrow Ni^- + CO$	1.76 ± 0.25	[95]
$Ni(CO)_2^- \rightarrow Ni(CO)_1^- + CO$	2.04 ± 0.25	[95]
$Ni(CO)_3^- \rightarrow Ni(CO)_2^- + CO$	1.23 ± 0.1	[95]
$Pt_3(CO)_6^- \rightarrow Pt_3(CO)_5^- + CO$	1.45 ± 0.2	[96]
$Pt_3(CO)_5^- \rightarrow Pt_3(CO)_4^- + CO$	0.93 ± 0.15	[96]
$Pt_3(CO)_4^- \rightarrow Pt_3(CO)_3^- + CO$	0.85 ± 0.1	[96]
$Pt_3(CO)_3^- \rightarrow Pt_3(CO)_2^- + CO$	2.0 ± 0.2	[96]
$Pt_3(CO)_2^- \rightarrow Pt_3(CO)_1^- + CO$	2.1 ± 0.5	[96]
$Pt_3(CO)_1^- \rightarrow Pt_3^- + CO$	2.2 ± 0.3	[96]

Some selected binding energies of carbonyls determined by collision induced fragmentation. All values are given in eV.

2.3.3. Binding energies

There are not many experimental data on the binding energies of a CO molecule bound to a bare metal cluster or an unsaturated complex. The most accurate values are determined using collision induced fragmentation [95,96]. The results of such experiments on $Ni_1(CO)_m^-$ and $Pt_3(CO)_m^-$ are listed in Table 3. The most interesting observation is the difference in binding energy of the first three COs ($m = 1-3$) bound to a Pt_3^- cluster compared with the latter three ($m = 4-6$) up to saturation. The binding energy of the first three COs is about twice the value of the other ones. These COs are assigned to bridge bound species, while the $m = 4-6$ ones are assigned to on-top sites. On a Pt surface [28,31,34] the binding energies of these two sites are about similar and approach the values measured for on-top bound COs in $Pt_3(CO)_m^-$ ($m = 3-6$).

2.4. Theoretical descriptions of the bonding in carbonyls

2.4.1. Valence electron counting rules

The observation of many stable complexes with a fixed number of valence electrons resulted in the development of the valence electron

counting rules [53,62–64,81]. For mononuclear compounds as $Ni(CO)_4$ (10 electrons per Ni atom and 2 per CO molecule) and $Cr(CO)_6$ (6 electrons per Cr atom) this number is 18 electrons. For some trinuclear complexes it is 48 electrons as in $Fe_3(CO)_{12}$. As origin of these counting rules it is assumed, that the metal core has a certain number of available valence orbitals, which are usually the valence d, p and s orbitals corresponding to a total number of 9 orbitals. Depending on the geometry of the metal core these are divided into bonding, non-bonding and antibonding orbitals. The antibonding orbitals are unoccupied. For example, according to Hückel calculations in a M_3 cluster 3 of the 3 × 9 orbitals are antibonding leaving 24 orbitals (= 48 electrons) [97]. The chemisorption process alters the energetic ordering of the remaining orbitals. It is assumed, that for each CO one of the 24 orbitals interacts with the CO 5σ orbital forming a bonding–antibonding pair of orbitals. Basically, one of the metal orbitals is destabilized and the CO 5σ orbital is stabilized. Accordingly, the number of orbitals available for the valence electrons of the metal (for Fe there are 8 electrons per atom corresponding to 12 occupied orbitals for Fe_3) decreases by one per ligand. The carbonyl is stable, if the number of remaining bonding and non-bonding metal orbitals (= 24 minus one per additional ligand in our example) is equal to half the number of metal valence electrons (12 orbitals for the 24 electrons of Fe_3). Therefore, saturation takes place at 12 CO ligands for Fe_3. The main conclusions for saturated carbonyls are as follows.

1. The interaction of the ligands with the metal core is delocalized and must be described by molecular orbitals.
2. Chemisorption causes a separation of the cluster orbitals into a bonding and antibonding manifold of orbitals forming a closed shell molecule.
3. The saturation limit depends on the geometry of the metal core, because it determines how many orbitals are strongly antibonding in the bare metal cluster. Each CO ligand destabilizes one additional metal d orbital.

In the literature we found no predictions of the properties of unsaturated carbonyls, whether there is just a smaller HOMO–LUMO gap or a more fundamental change in the electronic structure. The counting rules do not distinguish between different metals, except that in some cases (e.g. Pt) some of the atomic p orbitals are deemed "not available for interaction" thus effectively reducing the number of electrons for saturation. This is offered as an explanation for the stability of $Pt_3(CO)_6^{2-}$ with 44 electrons only.

2.4.2. Molecular orbital calculations

Pacchioni et al. [53,56,64,76] studied the chemisorption of CO on Ni clusters and predict a change of the configuration of the Ni atoms from d^9s to d^{10} as a result of CO chemisorption (Fig. 2). The metal 4s/p-derived orbitals are destabilized by the repulsive interaction with the diffuse CO 5σ orbitals. In small clusters all Ni atoms undergo the configuration change resulting in a non-magnetic molecule. In larger clusters the inner Ni atoms may remain in a d^9s configuration, because chemisorption influences largely the surface metal atoms. The uppermost density of occupied states in the neutral saturated carbonyls is dominated by metal d states. The LUMO of the saturated cluster has a predominant CO 2π and metal p character. The electronic structures of a carbonyl and a surface covered with CO are basically similar with one major difference: in the small bare clusters the bonding is due to the metal s/p orbitals. The metal 3d orbitals are highly localized and almost non-interacting. Upon CO adsorption the metal–metal bonding mechanism changes: the orbitals with a predominant metal s/p character are destabilized and shifted above the HOMO–LUMO gap. The 3d-derived levels are fully occupied (Figs 1 and 2), but more delocalized owing to the interactions (CO 5σ–metal d_{z^2} and

CO 2π–metal d_π) with the CO orbitals. These more delocalized 3d-derived orbitals now contribute significantly to the metal–metal bonding [56].

A detailed calculation [60] on $Pt_3(CO)_6^{2-}$ supports the picture given by Pacchioni et al. There are 15 Pt 5d-derived orbitals covering the range between 6.5 and 8.8 eV binding energy (BE) (with respect to the vacuum level). The 18 CO $1\pi/5\sigma$ derived orbitals are located between 12 and 13.8 eV (BE). The LUMO of the neutral cluster is the lowest of the manifold of CO 2π-derived orbitals located at 5.4 eV BE corresponding to a HOMO–LUMO gap of 1.2 eV. The next unoccupied orbital is about 1 eV higher in energy. Most of the calculations [53,56,60, 64,76] agree that the LUMO of a carbonyl cluster is an extraordinary stable CO 2π-derived orbital.

2.5. *Metal clusters ligated with CO*

The reaction rates of neutral and ionic clusters versus CO have been studied using a fast flow reactor [78,80–83] or a selected ion drift tube [77,79]. Two sets of data can be determined using these techniques: the reactivity of the bare metal cluster versus CO and the saturation limits. In a pioneering experiment Fayet at al. [77] determined the CO saturation limits of Ni_n^+ ions and interpreted the data using valence electron counting rules. A good agreement with the predictions from Lauher has been found, if appropriate geometries of the metal clusters are assumed. Cox et al. [78] determined the reactivity of small neutral Ni, Pd and Pt clusters versus CO. Pd is found to be more reactive than Ni and Pt and there is only a smooth size dependence of the reactivity of the Ni, Pd and Pt clusters.

Guo et al. [79] studied the CO uptake of Co_n^+ cluster cations using a selected ion drift tube and found a good agreement with the predictions of Lauher, if certain geometries of the clusters are assumed. Hintz et al. [81] studied the reaction of Ni_n^-, Pd_n^- and Pt_n^- cluster anions versus CO for $n > 2$. They found a smooth dependence of the reactivities on the cluster size and approximately similar saturation limits for Ni_n^-, Pd_n^- and Pt_n^- clusters of the same size ($\pm$ 1 or 2 CO ligands). Ni_n^- clusters always show the highest uptake of CO, while for Pt_n^- clusters the saturation limits are generally lower. Pd_n^- clusters seem to be an intermediate case. In detail, the size dependencies are rather irregular except for the trimer anions which all saturate at $m = 6$. The differences in the saturation limits are attributed to differences in the assumed geometries of the clusters. The lower limits found for $Pt_n(CO)_m^-$ clusters are explained by their presumably more compact structures compared with the $Ni_n(CO)_m^-$ clusters. Similar studies [83] using N_2 (N_2 has the same number of valence electrons as CO) resulted in much lower saturation limits (e.g. $Ni_3(N_2)_3^-$, $Pd_3(N_2)_2^-$ and $Pt_3(N_2)_3^-$).

Our photoelectron spectra of $Ni_n(CO)_m^-$, $Pd_n(CO)_m^-$ and $Pt_n(CO)_m^-$ clusters presented here reveal fundamental differences in the electronic structure of the non-saturated anions of the three metals (see below). These differences might very well be responsible for the observed differences in the saturation limits, independent of the geometry of the metal cores.

2.6. *Photoelectron spectroscopy of anions*

The application of any standard technique to clusters encounters the problem of mass separation. Therefore, most of the recent experiments deal with positive or negative ions. In the case of photoelectron spectroscopy, the use of anions [84–89] has the following three advantages.

1. The ions can easily be mass separated.
2. The spectra contain information about the final state, which is the neutral one in the case of the anion. Especially the vibrational modes of the neutral ground state can be determined.
3. If the neutral cluster is a closed shell species, the additional electron occupies the LUMO of

the neutral. Therefore, from the spectrum it can be deduced whether the neutral is a closed shell species. Furthermore, the size of the HOMO–LUMO gap can be determined.

Therefore, photoelectron spectroscopy of anions (PESa) [84–89] has proven to be a powerful tool in the studies of bare clusters. So far, there are only very few applications of PESa to ligated metal clusters. The anions are generated by attaching electrons to stable saturated mononuclear carbonyls ($Fe(CO)_5$ [88], $Cr(CO)_6$ [89], $Mo(CO)_6$ [89], $W(CO)_6$ [89] and $Ni(CO)_4$ [87]) resulting in the generation of various negatively charged fragments. (The saturation limit of a negatively charged mononuclear carbonyl is usually lower by one.) Nakajima et al. [88] generated negatively charged clusters of $Fe(CO)_5$ units of the type $((Fe(CO)_5)_n(Fe(CO_4))^-$. The photoelectron spectra of these Van der Waals bound species show no fine structure.

Stevens et al. [87] found the spectra of $Ni(CO)_m^-$ with $m = 1-3$ to be similar. The spectrum of $Ni(CO)_1^-$ exhibits a single intense feature at low BE (0.7–1.0 eV) with a vibrational fine structure corresponding roughly to the C–O stretch frequency of neutral $Ni(CO)_1$ (Table 2). According to the analysis of $Ni(CO)_1^-$ from Bauschlicher et al. [68] the additional electron occupies an Ni 4s/p-derived orbital and the single feature at low BE is assigned to photodetachment from this orbital. The vibrational fine structure indicates a weak admixture of CO 2π character of this orbital, because the CO bond length is altered by the detachment process. The spectrum of $Ni(CO)_1^-$ exhibits a second feature at higher BE (2.1 eV), which can be assigned to detachment from a Ni 3d orbital.

We did not succeed in generating $Ni(CO)_1^-$ using our method of exposing Ni_1^- to CO. However, we reproduced the spectrum of the saturated $Ni(CO)_3^-$ with some additional resolved fine structure and will compare our analysis with the ones given by Stevens et al. [87] and Bauschlicher et al. [68].

3. Experimental set up

The experimental set up (Fig. 3) is described in detail elsewhere [85,86]. The cluster anions are produced by a laser vaporization source, in which metal vapour is generated by a high power laser pulse hitting a rod consisting of the bulk metal. A carrier gas (He) flushes the metal plasma through an extender and a conical nozzle into vacuum. The Helium is provided from a pulsed valve for a duration of approximately 0.5 ms at a stagnation pressure of about 20 bar. Within the first few millimetres of the extender the clusters grow and are thermalized to approximately room temperature. About 4 cm downstream CO is added to the He. The CO valve is also an electromagnetically pulsed one with an opening duration of 0.2–1 ms and a CO stagnation pressure of about 2 bar. Varying the opening duration of the CO valve the amount of CO diluted in the He can be varied over a wide range. This set up is basically similar to the fast flow reactors used in various experiments determining reaction rates [78,80–83]. However, since we are not interested in the quantitative determination of the reaction rates, we have no means to measure the partial pressures of He, CO and the amount of metal clusters in the extender. The parameters are chosen to obtain the

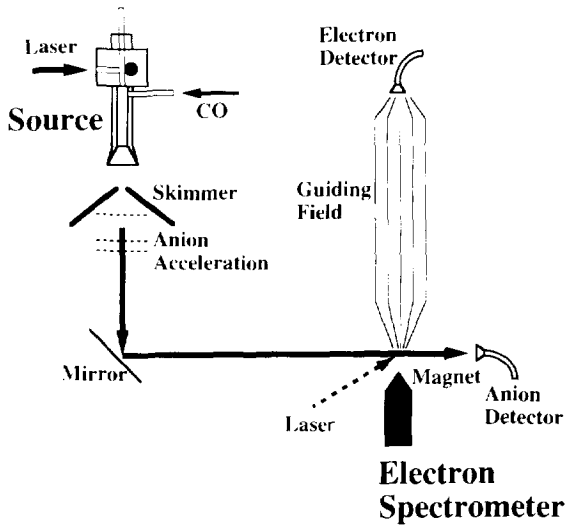

Fig. 3. Experimental set-up.

maximum amount of the species to be studied. Recently, a similar set up was used by Hintz et al. [81] to study the uptake of CO on Ni_n^-, Pd_n^- and Pt_n^- clusters quantitatively. It turned out to be necessary to use an extremely long extender to achieve saturation with CO for the larger clusters with $n > 4$. In our experiment, the maximum length of the extender was 15 cm and no saturation of the larger clusters could be achieved.

After passing the skimmer the negatively charged clusters are accelerated in a pulsed electric field. Depending on their time-of-flight (ToF) the clusters separate into a chain of bunches of defined cluster size. The anion beam is directed into the source region of a "magnetic bottle" ToF electron spectrometer. A selected bunch is irradiated by a laser pulse of a certain photon energy and the detached electrons are guided by magnetic fields through a drift region towards an electron detector. The binding energy (BE) is given by the difference between the photon energy and the kinetic energy of the electrons as determined by their ToF. The energy resolution depends on the kinetic energy of the electrons and the kinetic energy of the anions (Doppler broadening) and varies between 10–50 meV in the spectra presented here. The absolute calibration of the BE scale is uncertain by ± 30 meV.

4. Results and discussion

4.1. Mass spectra

The time-of-flight mass spectrometer is designed to obtain a maximum anion intensity. This is necessary for the spectroscopy of rare species (e.g. the unsaturated ligated metal clusters) obtaining a high energy resolution. Unfortunately, it corresponds to a low mass resolution ($m/\Delta m \approx 30$) and restricts our experiment to the study of the relatively small clusters. In the following we discuss some selected mass spectra of the bare and ligated clusters. The relative intensities of the individual features depend strongly on the parameters of the source (laser power, He stagnation pressure, CO stagnation pressure, timing). Therefore, the spectra shown are examples and some of the photoelectron spectra, especially those of the very small clusters, are obtained using different source conditions.

4.1.1. Nickel

Fig. 4 displays a comparison of mass spectra of Ni_n^- clusters produced by the laser vaporization

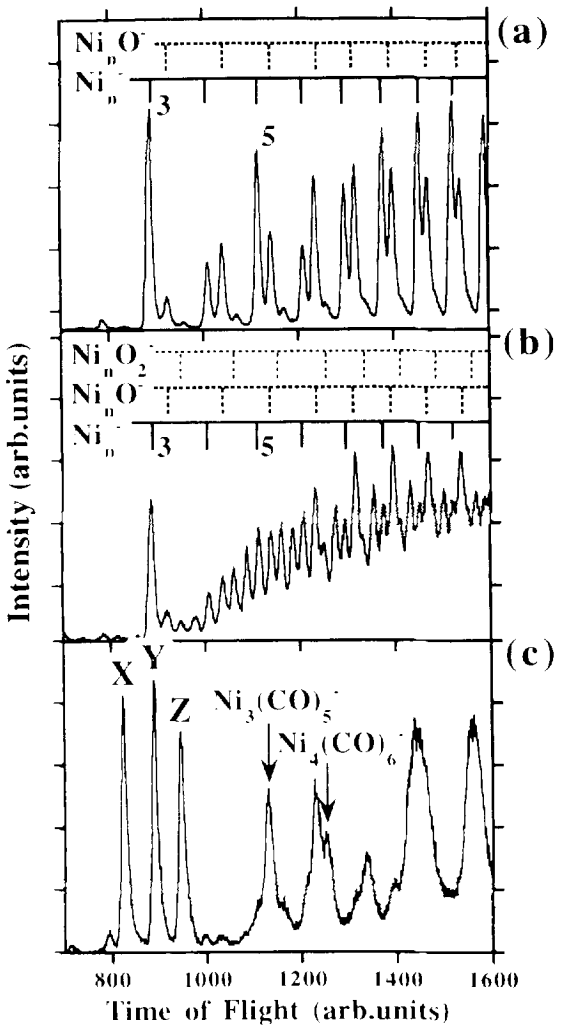

Fig. 4. Comparison of mass spectra of Ni_n^- clusters directly produced by a laser vaporization source (a) and the reaction products after introducing a small (b) and the maximum attainable amount of CO. For an assignment of the peaks see text.

source (a) and the reaction products after introducing a small (b) and the maximum attainable amount (c) of CO. The positions of the peaks assigned to the series of the bare Ni_n^- and the $Ni_nO_1^-$ clusters are indicated in Fig. 4(a). The first intense peak is assigned to Ni_3^-. The relative intensities of the monomer and dimer are much smaller and depend strongly on the source conditions. The oxides appear with a relatively high intensity even if the source has been run at very clean conditions for a longer period of time. If CO is introduced for a short moment into the source, the intensity of the oxides increases immediately and again decreases only slowly with time. Probably, part of the CO diffuses into the vaporization region and is dissociated in the laser plasma. As a result, the metal rod surface is covered with oxide and to a smaller amount with NiC. These impurities make an analysis of the spectra of the ligated clusters difficult. In addition, the mass of Ni (58.7 amu) is approximately twice the mass of CO (28 amu), which results in ambiguities assigning the photoelectron spectra (e.g. $Ni_2(CO)_4^-$ = 229.4 amu and $Ni_3(CO)_2^-$ = 232.1 amu) because of the limited mass resolution.

The spectrum of the $Ni_n(CO)_m^-$ generated with a small amount of CO (Fig. 4(b)) shows a multitude of partially overlapping peaks. The most intense features at higher ToF are assigned to $Ni_nO_1^-$ clusters, but $Ni_nO_2^-$, $Ni_nO_3^-$ and bare Ni_n^- can also be identified.

The spectrum of the $Ni_n(CO)_m^-$ obtained at the maximum CO pressure (Fig. 4(c)) shows three narrow peaks (X, Y, Z) corresponding to a relatively small mass and a series of broad peaks for larger cluster sizes. We were not able to unambiguously assign the three intense peaks (X, Y, Z). The best tentative assignments are $NiC(CO)_3^-$, $NiC(CO)_4^-$ and $NiC(CO)_5^-$. The broad peaks at larger cluster sizes can be assigned to metal cores with a certain number of adsorbed COs, but there are certainly contributions from various $Ni_nC_mO_k^-$ clusters. The calculated times of flight of $Ni_3(CO)_5^-$ and $Ni_4(CO)_6^-$ are indicated in the figure.

4.1.2. Palladium

Fig. 5 displays a comparison of mass spectra of bare Pd_n^- clusters (a) and the reaction products after introducing a small (b) and the maximum attainable amount (c) of CO. The mass spectrum of the bare Pd_n^- clusters exhibits almost no contributions from oxides or other impurities. At the adjustment of the source chosen in Fig. 5(a) the monomer and dimer are very weak and the first intense feature is assigned to Pd_4^-. If a small amount of CO is introduced into the extender,

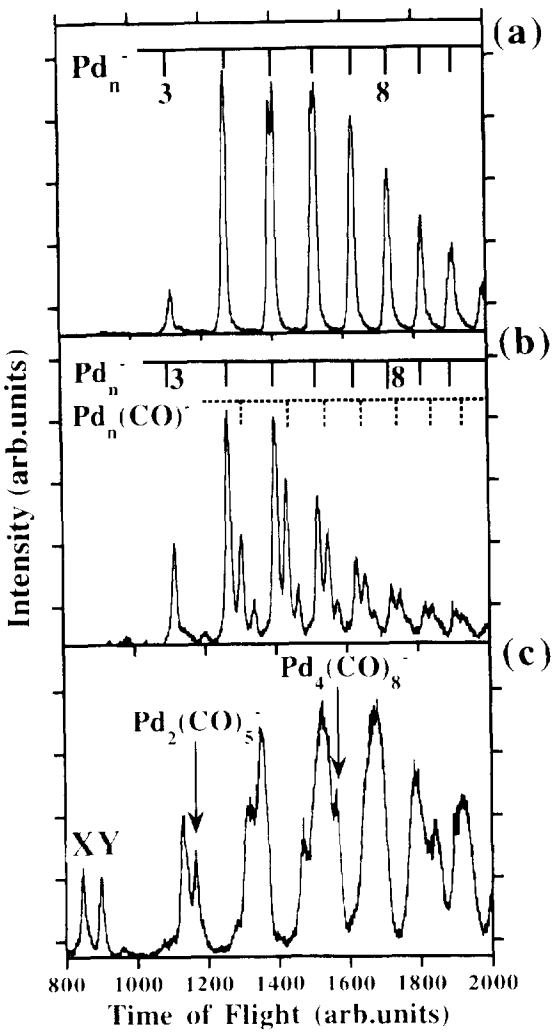

Fig. 5. Comparison of mass spectra of Pd_n^- clusters directly produced by a laser vaporization source (a) and the reaction products after introducing a small (b) and the maximum attainable amount (c) of CO. For an assignment of the peaks see text.

additional peaks corresponding to $Pd_n(CO)_1^-$ (indicated in Fig. 5(b)) and $Pd_n(CO)_2^-$ appear. This spectrum is very similar to the one published in Ref.78. At high CO pressure (Fig. 5(c)) broad peaks are observed corresponding to Pd_n^- clusters with a high number of adsorbed CO molecules (e.g. peaks assigned to $Pd_2(CO)_5^-$ and $Pd_4(CO)_8^-$ are marked in Fig. 5(c)). For Pd_n^- with $n = 2,3,4$ and 5 we observe a maximum uptake of $m = 5, 6, 8$ and 9 CO molecules, respectively, in agreement with the measurements of Hintz at al. [81]. For the larger Pd clusters we were not able to achieve saturation.

Similar to the case of Ni_n^- there are two narrow peaks at small cluster size (X, Y) in the mass spectrum at high CO pressure, which we could not unambiguously assign. Possible assignments are $PdC(CO)_2^-$ and $PdC(CO)_3^-$, respectively.

4.1.3. Platinum

Fig. 6 compares ToF mass spectra of bare (a) and ligated Pt_n^- clusters (b, c). The most intense features in the spectrum of the bare clusters are assigned to Pt_n^- for $n = 1$ and 3–7. The relative intensity of bare Pt_2^- is smaller than the one of Pt_2O^-. All bare cluster mass peaks are accompanied by weak features (shoulders at larger ToF) corresponding to $Pt_nO_m^-$ and $Pt_nC_m^-$ compounds. At low CO pressure (Fig. 6(b)) reaction products with a varying number of adsorbed COs are observed for all clusters. In the case of $Pt_3(CO)_m^-$ m varies between $m = 0$–6. In contrast, at this particular CO pressure only one predominant reaction product ($Pt_4(CO)_6^-$) is found for Pt_4^-. Non-dissociative chemisorption of CO is the dominant reaction except for the atom and the dimer. For both, Pt_1^- and Pt_2^- features assigned to various compounds $Pt_nO_mC_k^-$ are identified. In Fig. 6(c) the clusters have reacted with the maximum amount of CO attainable in our experiment. For $Pt_3(CO)_m^-$ now the saturated carbonyl anion $Pt_3(CO)_6^-$ is the most intense peak of the $Pt_3(CO)_m^-$ series. For all larger clusters the broad mass distributions narrow down to maxima corresponding to the saturated metal clusters. For

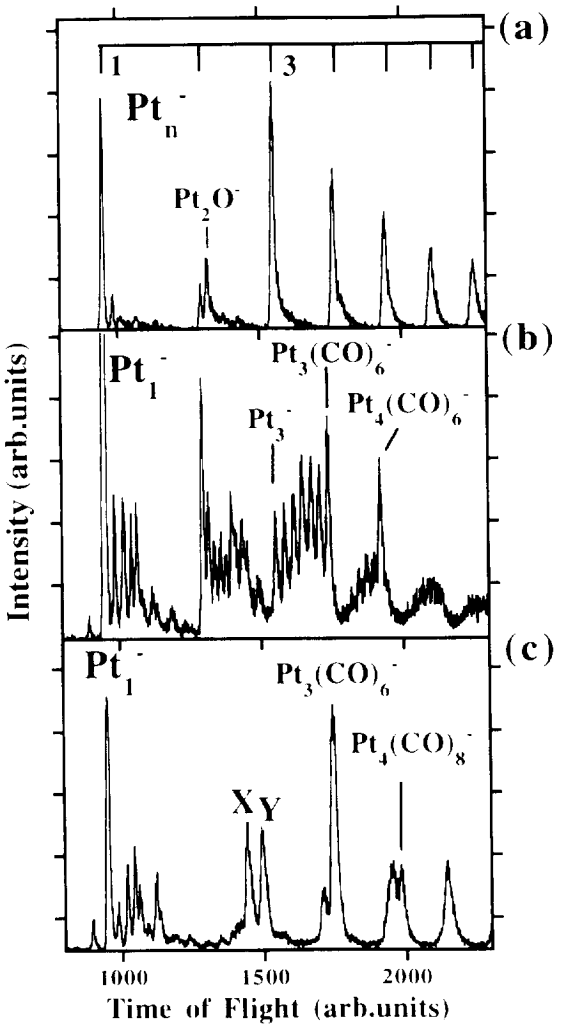

Fig. 6. Comparison of mass spectra of Pt_n^- clusters directly produced by a laser vaporization source (a) and the reaction products after introducing a small (b) and the maximum attainable amount (c) of CO. For an assignment of the peaks see text.

Pt_n^- with $n = 3$, 4 and 6 we find saturation limits of $m = 6$, 8 and 9 CO molecules in agreement with the measurements of Hintz et al. [81]. The peaks marked X and Y cannot be assigned unambiguously. In Fig. 6(c) Pt_1^- is the only bare metal cluster observed and all other Pt_n^- are totally depleted by chemisorption reactions.

4.2. Photoelectron spectra

We start the discussion with the data on the

electronic structure of the $Pt_n(CO)_m^-$ clusters, which can be readily interpreted on the basis of a simplified version of the Blyholder model (Fig. 1) [53,76]. The interaction of the CO 5σ with the metal d_{z^2} orbitals is neglected. There is a interaction between the metal s/p and CO 5σ orbitals. Owing to chemisorption the metal s/p derived orbitals are strongly destabilized and the configuration of the metal atoms changes with increasing CO uptake from d^9s to d^{10} (Fig. 2). The CO 2π orbitals interact with the metal d orbitals resulting in a stabilization of the latter ones. The metal atom assumes a closed shell configuration. This approach is in agreement with our findings of a transition from an open-shell to a closed-shell owing to saturation with CO (see below). Finally, a similar ordering of orbitals has also been found in recent high level calculations on certain platinum and nickel carbonyls [58,60].

For the interpretation of the $Ni_n(CO)_m^-$ spectra a correction has to be introduced owing to correlation effects. Finally, we will show the results of the $Pd_n(CO)_m^-$ clusters, which seem to be an intermediate case between Ni and Pt. In general, the discussion is focused on two topics: First of all the electronic structure in comparison with the Blyholder model and second the vibrational information, which is related to the geometry, in comparison with surface adsorption data.

4.2.1. The electronic structure of the ligated metal clusters

In the present contribution we refrain from a discussion of the spectra of the bare metal clusters. A detailed analysis of the Ni_n^-, Pd_n^- and Pt_n^- data with $n = 1-15$ will be given elsewhere [98]. The spectra of the dimers and trimers agree with earlier measurements [93,99,100]. The vertical detachment energies are listed in Table 4.

4.2.1.1. Platinum. For the clusters with more than $n = 4$ Pt atoms we were not able to generate the saturated species, because the reaction rates are too low in relation to the parameters of our experiment (maximum attainable CO partial pressure, maximum exposure time in the extender). The spectra of the unsaturated $Pt_n(CO)_m^-$ *clusters with* $n > 4$ *do not show any pronounced structures. The following discussion focuses on the* $Pt_n(CO)_m^-$ *species with* $n = 1-4$.

4.2.1.1.1. $Pt_3(CO)_m^-$, $Pt_4(CO)_m^-$. Figs 7 and 8 show series of photoelectron spectra of $Pt_3(CO)_m^-$

Table 4
Vertical detachment energies extracted from photoelectron spectra

	Pt				Ni			Pd	
	1	2	3	4	1	2	3	2	3
0	2.1 (0.1)	1.9 (0.1)	1.9 (0.1)	2.6 (0.1)	1.2 (0.1)	1.0 (0.1)	1.4 (0.1)	1.7 (0.1)	1.5 (0.1)
1		1.9 (0.3)	2.5 (0.2)	2.4 (0.2)		1.1 (0.1)	1.6 (0.1)	1.0 (0.1)	1.5 (0.2)
2			2.5 (0.5)	2.5 (0.3)				1.4 (0.1)	1.7 (0.1)
3	1.3 (0.1)		2.4 (0.3)	2.6 (0.3)	1.1 (0.1)		1.8 (0.2)	1.5 (0.2)	2.0 (0.2)
4		2.4 (0.2)	2.4 (0.3)	2.6 (0.3)		1.9 (0.1)	1.9 (0.3)	1.4 (0.1)	1.7 (0.2)
5		1.9 (0.1)	2.4 (0.3)	2.6 (0.3)					1.7 (0.3)
6			2.4 (0.1)	2.7 (0.3)			2.4 (0.1)		1.9 (0.2)
7				2.8 (0.2)					
8				2.9 (0.2)					

The vertical detachment energies (VDEs) extracted from the photoelectron spectra of bare ($m = 0$) and ligated metal clusters. The line corresponds to the number of metal atoms (Pt: $n = 1-4$; Ni: $n = 1-3$, Pd: $n = 1,2$) and the row corresponds to the number of CO ligands ($m = 0-8$). All values are given in eV. If the spectra exhibit a distinct peak at emission threshold the position of the maximum of this peak is taken as the VDE. If the spectrum exhibits no maxima but an increasing emission signal above threshold the intersection of a straight line fitted to the emission signal with the zero line is taken as the VDE. The error given in parenthesis is a result of the experimental error, the limited signal to noise ratio and the uncertainty of the fit procedure.

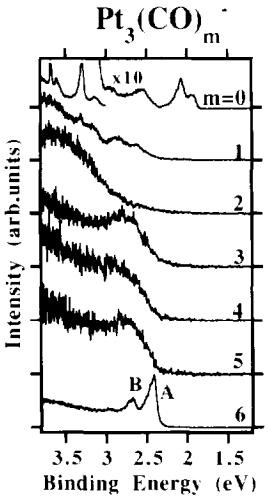

Fig. 7. Photoelectron spectra of $Pt_3(CO)_m^-$ for $m = 0$–6. The photon energy is $h\nu = 4.0$ eV.

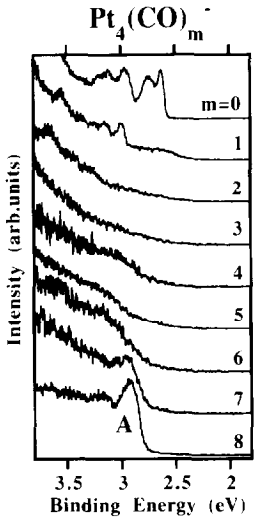

Fig. 8. Photoelectron spectra of $Pt_4(CO)_m^-$ for $m = 0$–8. The photon energy is $h\nu = 4.0$ eV.

for $m = 0$–6 and $Pt_4(CO)_8^-$ for $m = 0$–8, respectively. The spectra of the bare metal clusters exhibit various relatively sharp features corresponding to photoemission from the metal 6s/p and 5d-derived orbitals, while the spectra of the ligated, non-saturated clusters show a smooth featureless emission signal. Only the spectra of the saturated clusters ($Pt_3(CO)_6^-$, $Pt_4(CO)_8^-$) are different: at emission threshold pronounced peaks (marked A) appear. In the case of $Pt_3(CO)_6^-$ a vibrational fine structure corresponding to the stretch frequency of CO is resolved (see below).

Without further analysis these two series of spectra indicate that saturation is an electronic and not a steric effect, because the electronic structure of the saturated negatively charged species changes dramatically. The appearance of peak A can be explained in the framework of the Blyholder model (Figs 1 and 2). As long as the cluster is non-saturated there are unoccupied d-derived molecular orbitals, which can accommodate the additional electron of the negatively charged cluster. The smooth featureless emission signal in Fig. 7 for $m = 1$–5 and Fig. 8 for $m = 1$–7 is probably a superposition of photoemission from the various 5d-derived orbitals with a considerable broadening due to vibrational excitation (the excitation of the vibration of the CO molecule versus the metal core, see the discussion of the vibrational modes of $Ni_1(CO)_3^-$). In the saturated cluster the additional electron must occupy the LUMO (Fig. 2), which is either a Pt 6s/p or a CO 2π derived orbital (Fig. 1). Photoemission from such orbitals has a larger cross section at the low photon energies used in our experiment compared with photoemission from d-derived orbitals[1]. This explains the appearance of the pronounced peaks in the spectra of the saturated clusters, because in addition to the emission from the metal 5d band there is emission from the CO 2π hybrid orbital, which is unoccupied in the unsaturated clusters. We assign features A to detachment from a CO 2π hybrid orbital (and not the metal 6s/p), because the C–O stretch vibration is excited owing to photoemission from this orbital. If the electron

[1] At photon energies close to threshold the photoemission cross section is larger for atomic s and p orbitals than for d and f ones. This cross-section dependence [101] is quite often used in solid state physics to assign emission features. In the case of d and f orbitals this can be justified, because these orbitals are localized and not basically different from the ones of a free atom. For the strongly delocalized metal s (or σ) and p (or π) orbitals such an analogy is less valid. However, the CO 2π orbitals are relatively localized, too, and the shape of a π^* orbital is basically similar to two non-interacting C and O atomic p orbitals.

would occupy a metal 6s/p-derived orbital, no excitation of the C–O stretch vibration is expected. For symmetry reasons only the CO 5σ orbital can hybridize with this metal orbital and the CO 5σ orbital is non-bonding with respect to the C–O bond.

These qualitative assignments are in agreement with the results of calculations [60] of the energetic ordering of the single particle orbitals of $Pt_3(CO)_6^{2-}$. The 2 additional electrons occupy a 2π-derived a_2 orbital. In the neutral cluster the 15 uppermost occupied orbitals (30 electrons) are the ones derived from the metal 5d orbitals. There is a gap of 0.9 eV between the manifold of metal 5d orbitals and the lowest CO 2π orbital. From our photoemission data (Fig. 7) this gap seems to be smaller (< 0.5 eV). However, the determination of the gap is hampered by several problems. All features show a broadening due to vibrational excitation, which is not resolved for the metal d emission. Such broadening effects make it difficult to determine gaps in photoelectron spectra. In addition, the calculation refers to $Pt_3(CO)_6^{2-}$ and not to the neutral $Pt_3(CO)_6$ cluster (the gap measured in a photoelectron spectrum of an anion corresponds to the one of the neutral).

We conclude that the appearance of a pronounced peak A at emission threshold in the photoelectron spectra of the saturated $Pt_{3,4}(CO)_m^-$ clusters can be explained by the formation of a closed shell configuration of the saturated neutral species as described in Fig. 2. As we will show the observation of such a "2π peak" is not unique to this species.

4.2.1.1.2. $Pt_2(CO)_m^-$. Fig. 9 shows a series of spectra of $Pt_2(CO)_m^-$ with $m = 0,1,4,5$ similar to the data on Pt_3^- and Pt_4^- (Figs 7 and 8). The spectrum of bare Pt_2^- is discussed in detail in Ref.93. We were not able to record spectra of $Pt_2(CO)_m^-$ with $m = 2$, 3 owing to the low intensity of these species in the mass spectrum. Analogous to the unsaturated spectra of the $n = 3$, 4 series the spectrum of $Pt_2(CO)_1^-$ exhibits a relatively unstructured emission signal although

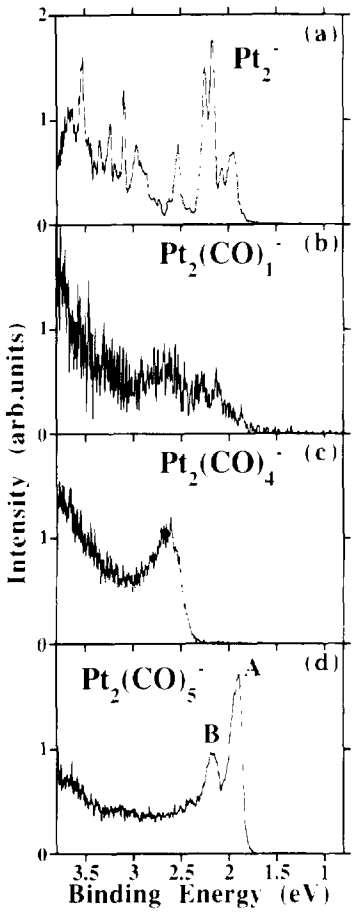

Fig. 9. Photoelectron spectra of $Pt_2(CO)_m^-$ for $m = 0$, 1, 4, 5. The photon energy is $h\nu = 4.0$ eV.

the low signal to noise ratio makes this conclusion rather uncertain. In the spectrum of $Pt_2(CO)_4^-$ (Fig. 9(c)) there is a broad relative intense feature at emission threshold, which exhibits no resolved vibrational fine structure. The spectrum of the saturated dimer (Fig. 9(d)) with 5 adsorbed CO molecules exhibits again the characteristic 2π peak A with a vibrational fine structure corresponding to the C–O stretch vibration (A,B). Incidentally, the saturation of Pt_2^- with 5 COs is not explained by any of the magic numbers of the "counting rules".

4.2.1.1.3. $Pt_1(CO)_m^-$. Fig. 10 displays the spectra of $Pt_1(CO)_m^-$ with $m = 0$, 3. We were not able to record spectra of $Pt_1(CO)_m^-$ with $m = 1$, 2 owing to problems in generation of these species

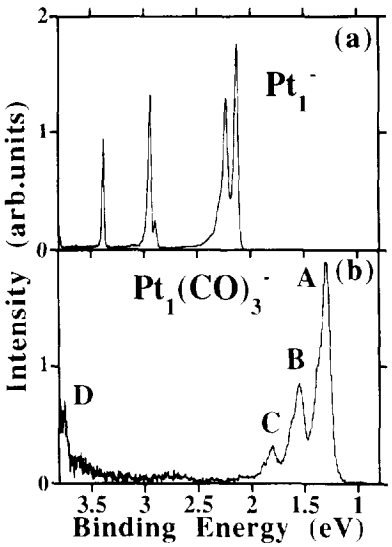

Fig. 10. Photoelectron spectra of $Pt_1(CO)_m^-$ for $m = 0, 3$. The photon energy is $h\nu = 4.0$ eV.

with sufficient intensity. The spectrum of the bare atom shows relatively sharp peaks corresponding to transitions from the anion electronic ground state into the neutral ground and excited states. The width of these peaks corresponds to the experimental resolution, which increases with increasing binding energy (= decreasing kinetic energy) [86].

$Pt_1(CO)_3^-$ corresponds to the saturation limit of the negatively charged mononuclear carbonyl. For the neutral, the stable carbonyl is $Pt_1(CO)_4$. In general the saturation limits of negatively charged clusters are either lower or equal to the ones of the neutrals [81]. $Pt_1(CO)_4^-$ is probably unstable to dissociation into $Pt_1(CO)_3^-$ + CO similar to $Ni_1(CO)_4^-$ [87]. The photoelectron spectrum of $Pt_1(CO)_3^-$ exhibits the characteristic 2π peak A with the vibrational fine structure corresponding to the CO stretch frequency (A, B, C). Since the neutral $Pt_1(CO)_3$ is an unsaturated cluster, this is in contradiction to our interpretation of the data of the larger $Pt_n(CO)_m^-$ clusters, where the peak appears in case the neutral is a closed shell saturated carbonyl.

This discrepancy can be explained by correlation effects. A 2π peak has also been observed previously in the spectra of $Ni_1(CO)_1^-$, $Ni_1(CO)_2^-$ and $Ni_1(CO)_3^-$ [87] and appears in all spectra of the $Ni_n(CO)_m^-$ clusters shown below. Obviously, our simple picture of the formation of a closed shell causing the additional electron to occupy a different orbital fails for Pt_1^- and Ni_n^- clusters. These species have highly localized d orbitals for which the single particle picture has deficiencies. In the Pt atom the 5d orbitals are localized and in Ni clusters and even bulk Ni the 3d orbitals are also localized giving rise to the ferromagnetic properties. In larger Pt clusters and even Pt_2 the 5d orbitals start to delocalize and contribute to the bonding in the cluster [93]. In a delocalized orbital correlation effects are reduced, because the electrons have a larger average distance. An additional electron generally prefers a delocalized orbital to minimize the Coulomb repulsion by the other electrons. For example, if in a neutral $Ni_n(CO)_m$ cluster there is an unoccupied relatively stable but highly localized 3d orbital, an additional electron might prefer the delocalized CO 2π derived orbital. Such correlation effects are reflected in the energies of the different configurations of the isolated Ni atom: although the 4s and 3d orbitals are energetically almost degenerate, the d^{10} configuration is higher in energy by about 1.7 eV with respect to the d^9s configuration [93,99]. This energy is characteristic for the strength of the Coloumb repulsion experienced by the 10th electron in the 3d orbital.

Only in $Pt_n(CO)_m$ clusters with $n > 1$ such effects are so small, that a straightforward interpretation using the single particle picture seems possible. The reason for the smaller influence of correlation effects in Pt clusters is the larger size of the 5d orbitals resulting in larger overlap and higher degree of delocalization of the 5d electrons. Otherwise the concept of a shell closing effect is irrelevant. Nevertheless, the mechanism of saturation might be of similar origin for neutral $Pt_n(CO)_m$ and $Ni_n(CO)_m$ clusters despite the differences in electron correlation. While the photoelectron spectra of bare Ni_n^- and Pt_n^- clusters exhibit large differences, the ones of the

corresponding saturated carbonyls show large similarities (see below).

In general, differences in the saturation limits of neutral and charged species cannot be explained using our simple model for saturation. We know of no simple explanation on the level of the Blyholder model for the instability of $Pt_1(CO)_4^-$. A more sophisticated approach involving the total energies seems necessary.

In terms of the electron counting rules the additional electron counts as half a CO ligand explaining the lowering of the saturation limit in a straightforward manner. However, this approach cannot explain the cases when the limits are equal for the neutral and negatively charged species (e.g. $Pt_3(CO)_6$).

4.2.1.2. Nickel

4.2.1.2.1. $Ni_3(CO)_m^-$. Owing to the limited mass resolution we are not able to assign a spectrum unambiguously to a certain cluster for the Ni data. Fig. 11 shows a series of spectra tentatively assigned to $Ni_3(CO)_m^-$ with $m = 0$, 1, 3, 4 and 6. For the even m the assignment is uncertain, e.g. the spectrum of $Ni_3(CO)_6^-$ could also be assigned to $Ni_4(CO)_4^-$, if the analysis is based on the mass only. However, there is

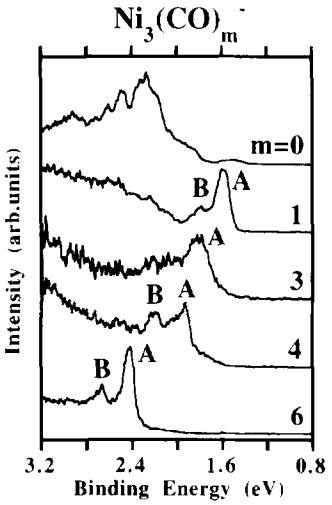

Fig. 11. Photoelectron spectra of $Ni_3(CO)_m^-$ for $m = 0$, 1, 3, 4, 6. The photon energy is $h\nu = 4.0$ eV.

additional information to assign a spectrum: (i) the vertical detachment energy (VDE, Table 4) in a series assigned to a certain metal core is expected to increase monotonically with increasing m; (ii) the spectra of the saturated clusters are recorded at high CO pressure and (iii) if the feature at emission threshold exhibits a vibrational fine structure corresponding to the energy of the C–O stretch vibration, we consider an assignment to other compounds as, e.g. $Ni_nO_m^-$ or $Ni_nC_m^-$ to be unlikely.

In contrast to the $Pt_3(CO)_m^-$ series (Fig. 7) all spectra of the $Ni_3(CO)_m^-$ clusters exhibit a 2π peak A with a vibrational fine structure corresponding to the excitation of the C–O stretch vibration (A, B). While the spectra of $Ni_3(CO)_3^-$ and $Ni_3(CO)_4^-$ exhibit poor statistics and show a less pronounced fine structure, the spectrum of $Ni_3(CO)_1^-$ clearly shows the characteristic progression. As in the case of $Pt_1(CO)_3^-$ (see above) we explain the appearance of this peak in the spectra of the unsaturated $Ni_n(CO)_m^-$ clusters as an effect of the high degree of localization of the valence d orbitals.

Despite the differences in the spectra of the unsaturated $Pt_3(CO)_m^-$ and $Ni_3(CO)_m^-$ clusters caused by the correlation effects we consider the chemisorption mechanism of the two metals to be basically similar. Fig. 12 shows a comparison of the photoelectron spectra of the bare Ni_3^- and Pt_3^- and saturated $Ni_3(CO)_6^-$ and $Pt_3(CO)_6^-$ clusters. There is a striking similarity of the spectra of the latter ones, especially, if the differences in the spectra of the bare clusters are taken into consideration. For $Pt_3(CO)_6^{2-}$ and $Ni_3(CO)_6^{2-}$ such a similarity of the electronic structure has been predicted by theory [60].

4.2.1.2.2. $Ni_2(CO)_m^-$. Fig. 13 displays a comparison of photoelectron spectra of Ni_2^-, $Ni_2(CO)_1$ and $Ni_2(CO)_4^-$. The assignment of the spectrum of $Ni_2(CO)_4^-$ is uncertain and it might alternatively be assigned to $Ni_3(CO)_2^-$. However, the latter assignment seems unlikely, because the spectrum shown is recorded at high CO pressure and exhibits a rather strong 2π peak. Also, the

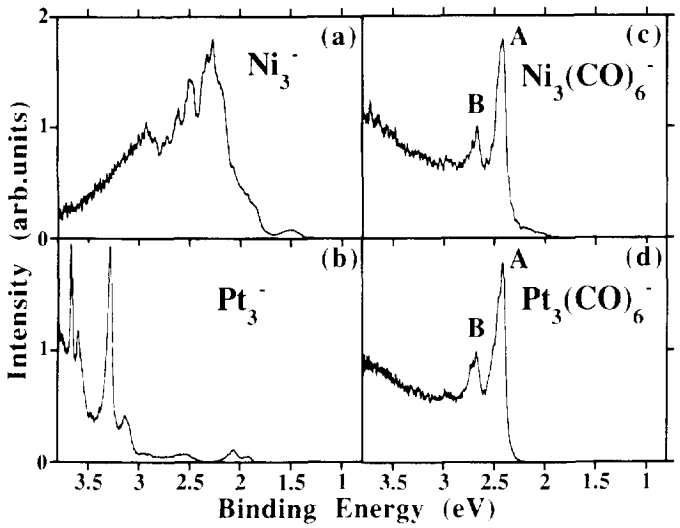

Fig. 12. Comparison of the photoelectron spectra of bare Ni_3^- and Pt_3^- with the saturated species $Ni_3(CO)_6^-$ and $Pt_3(CO)_6^-$ in the binding energy range 1.5–3.5 eV. The photon energy is $h\nu$ = 4.0 eV.

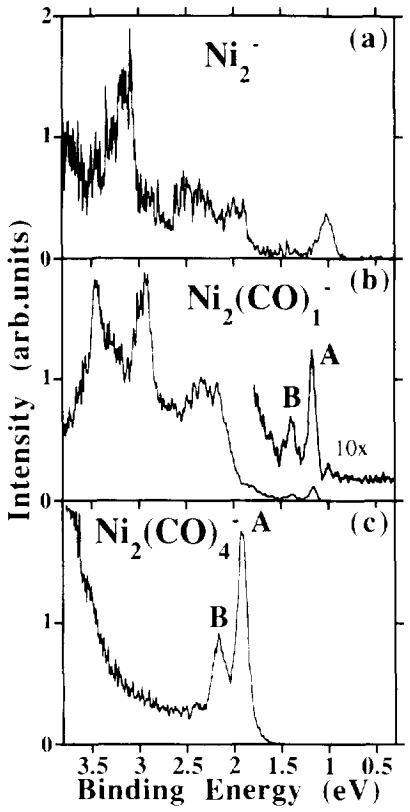

Fig. 13. Photoelectron spectra of $Ni_2(CO)_m^-$ for m = 0, 1, 4. The photon energy is $h\nu$ = 4.0 eV.

VDE (Table 4) of this species does not fit into the $Ni_3(CO)_m^-$ series, because its VDE is higher than the one of $Ni_3(CO)_3^-$.

According to our assignment the saturation limit is lower for $Ni_2^-(m=4)$ than for $Pt_2^-(m=5)$. Hintz et al. [81] have found small differences in the saturation limits of Ni, Pd and Pt clusters. It is interesting, that despite the different saturation limits the photoelectron spectra of $Ni_2(CO)_4^-$ (Fig. 13(c)) and $Pt_2(CO)_5^-$ (Fig. 9(d)) are almost identical.

Feature A in the spectrum of $Ni_2(CO)_1^-$ is assigned to photoemission from the 2π orbital analogous to the other $Ni_n(CO)_m^-$ spectra although this feature has a low relative intensity. This assignment is supported by the observation of a second peak B with an energetic spacing corresponding to approximately the C–O stretch vibration (see below). The low relative intensity of this feature might be caused by a cross section effect beyond the simple general rule [101]. Another possible explanation is an electron signal from other, not completely resolved species (e.g. Ni_2C, Ni_2O; see Fig. 4(b)). These might contribute to the intense features at higher binding energies.

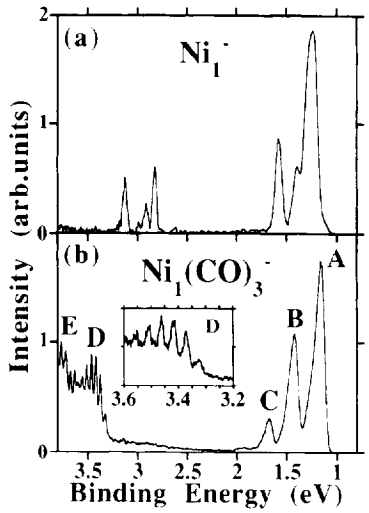

Fig. 14. Photoelectron spectra of $Ni_1(CO)_m^-$ for $m = 0, 3$. The photon energy is $h\nu = 4.0$ eV.

4.2.1.2.3. $Ni_1(CO)_3^-$. The spectrum of $Ni_1(CO)_3^-$ (Fig. 14(b)) is remarkably similar to the one of $Pt_1(CO)_3^-$ (Fig. 10(b)), although the spectra of the bare atoms differ considerably. Both exhibit a feature A at low BE ($Ni_1(CO)_3^- \approx 1.15$ eV; $Pt_1(CO)_3^- \approx 1.30$ eV) with a pronounced vibrational fine structure corresponding to the C–O stretch vibration. At high BE ($\approx$ 3.3–3.8 eV) there is a second feature, which is split into two peaks D and E for $Ni_1(CO)_3^-$. This similarity of the two spectra indicates, that there is only a minor contribution of photoemission from occupied metal s orbitals, because for the two metal atom anions the emission features of these orbitals (Ni 4s and Pt 6s) are located at totally different binding energies (Ni 4s:1.15 eV (Fig. 14(a)) and Pt 6s:2.13 eV (Fig. 10(a))). The reason is the relativistic contraction of the Pt 6s orbital. The small difference of the VDEs (Table 4) for $Ni_1(CO)_3^-$ and $Pt_1(CO)_3^-$ indicates, that the metal s orbitals are not occupied as predicted for saturated clusters (Figs 1 and 2). This explains also the general observation of similar spectra for saturated $Ni_n(CO)_m^-$ and $Pt_n(CO)_m^-$ clusters ($Pt_3(CO)_6^- \approx Ni_3(CO)_6^-$; $Pt_2(CO)_5^- \approx Ni_2(CO)_4^-$).

In the spectrum of $Ni_1(CO)_3^-$ feature D (insert in Fig. 14(b)) exhibits a vibrational fine structure with a frequency of 380 $\pm$ 30 cm^{-1}. This frequency is similar to the one of the vibration of a CO molecule versus a Ni surface (400 cm^{-1} [14]) and is therefore assigned to the vibration of the CO molecule versus the metal atom. The peak is assigned to emission from an orbital, which contributes to the chemisorption bond. However, no vibrational fine structure corresponding to the excitation of the C–O stretch vibration is observed. Peak E is assigned to a transition into a different electronic state because of its large separation ($>$ 2500 cm^{-1}) from feature D. Both D and E exhibit the same vibrational fine structure and are probably similar in their configurations. In this range of binding energies emission from metal d orbitals with an admixture from CO 2π orbitals is expected (Fig. 1). However, if the orbital corresponding to feature D has a contribution from CO 2π character, the excitation of the C–O stretch vibration is expected.

This discrepancy is resolved if peak D is due to photoemission from an orbital formed by the interaction of the metal d and the CO 5σ orbitals. Emission from such an orbital should result in the excitation of the low energy CO–metal vibration but not of the C–O stretch vibration, because the 5σ orbital is non-bonding with respect to the C–O bond. This interaction has been neglected so far for simplification (Fig. 1). The metal d_{z^2} orbital interacts with the CO 5σ orbital forming bonding ($5\sigma + d_{z^2}$) and antibonding ($d_{z^2} - 5\sigma$) hybrid orbitals [1,35,66]. The ($5\sigma + d_{z^2}$) mixing corresponds to a further shift of the CO 5σ orbitals to higher binding energies in addition to the stabilization caused by the CO 5σ–metal s interaction. The formation of an antibonding ($d_{z^2} - 5\sigma$) hybrid orbital has been predicted by theory but never been observed directly. For Ni and Pt this orbital should be occupied and located at the upper edge of the metal d band (lowest BE of the metal d-derived features in the PES) [1,66]. Peak D in the spectrum of $Ni_1(CO)_3^-$ can be assigned to detachment from the uppermost metal d orbital (see the discussion of $Pt_3(CO)_6^-$) and we therefore assign

this feature to emission from the (d_{z^2}–5σ) hybrid orbital. In agreement with the calculation from Bagus et al. [66] the orbital is occupied and thus in total the $5\sigma/d_{z^2}$ interaction is non-bonding for Ni.

The removal of an antibonding electron should result in an increase of the vibration frequency of the corresponding bond. However, in the final state of the transition corresponding to peak D there is one electron occupying an antibonding 2π hybrid orbital (so to speak the additional electron of the anion), which compensates for the increase in bond strength. Therefore, the observed frequency is probably similar to the one of the neutral ground state. This explains the similarity of the frequency to the one on a Ni surface.

4.2.1.3. Palladium

4.2.1.3.1. $Pd_3(CO)_m^-$. Fig. 15 displays the photoelectron spectra of $Pd_3(CO)_m^-$ clusters with $m = 0$–6. According to the measurements by Hintz et al. [81] the saturation limit of Pd_3^- is $m = 6$ in agreement with our observations. The spectrum of $Pd_3(CO)_6^-$ shows no pronounced 2π peak comparable to the spectra of $Ni_3(CO)_6^-$ and $Pt_3(CO)_6^-$, but the spectrum of $Pd_3(CO)_2^-$ exhibits

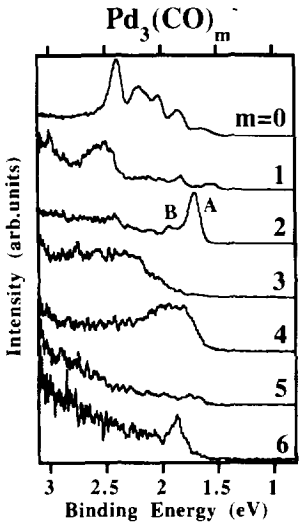

Fig. 15. Photoelectron spectra of $Pd_3(CO)_m^-$ clusters with $m = 0$–6. The photon energy is $h\nu = 4.0$ eV.

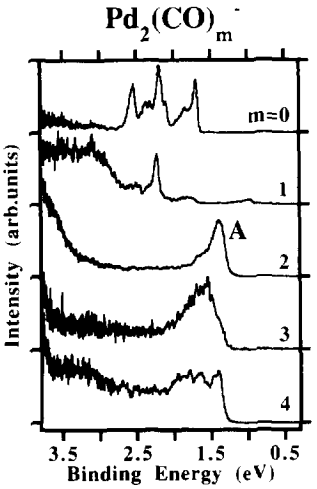

Fig. 16. Photoelectron spectra of $Pd_2(CO)_m^-$ clusters with $m = 0$–4. The photon energy is $h\nu = 4.0$ eV.

such a peak A with the characteristic vibrational fine structure. It is interesting, that the spectrum of $Pd_3(CO)_2^-$ is very similar to the one of $Ni_3(CO)_1^-$.

4.2.1.3.2. $Pd_2(CO)_m^-$. Fig. 16 shows the photoelectron spectra of $Pd_2(CO)_m^-$ clusters with $m = 0$–4. Again, there is a pronounced 2π peak in the spectrum of $Pd_2(CO)_2^-$ (marked A). The spectra of the clusters with 3 and 4 CO molecules exhibit a broad peak at emission threshold. According to the mass spectrum (Fig. 5(c)) $Pd_2(CO)_5^-$ is the saturated cluster. However, we did not succeed in recording a photoelectron spectrum from this carbonyl.

There are no stable Pd carbonyls known corresponding to, e.g., the $Pt_3(CO)_6^{2-}$ dianion [49]. A possible explanation is the preference of a d^{10} configuration of the Pd atoms in the small clusters. With increasing cluster size the average configuration approaches the bulk value $d^{8.7}s^{1.3}$ [94] similar to Ni and Pt. A d^{10} configuration corresponds to an electronic closed shell with a lower polarizability, i.e., a lower ability to form a bond with the ligand orbitals, which explains the lower binding energy of the ligands. However, the experimental determined saturation limits [81] seem to be unaffected by the weaker bond.

For both series of spectra of $Pd_n(CO)_m^-$ clusters

($n = 2,3$) we observe a pronounced 2π peak for $m = 2$ similar to the spectra of the saturated Pt carbonyls. For the other Pd carbonyls no such feature could be identified unambiguously, although the signal to noise ratio is rather low in some cases (e.g. the spectrum of $Pd_3(CO)_6^-$). This might indicate a special electronic structure of the species with 2 CO ligands. However, we know of no simple explanation for this effect.

4.2.2. Vibrational spectroscopy of the ligated metal clusters

Many of the photoelectron spectra discussed above exhibit a pronounced peak at emission threshold with a vibrational frequency corresponding roughly to the C–O stretch vibration. This 2π peak has been assigned to emission from an orbital having the character of the ligand 2π orbitals, which is the LUMO of the neutral cluster. The transition corresponding to this feature is the one into the neutral electronic ground state and the vibrational fine structure (''cold bands'') of this feature corresponds to excitations of modes of the neutral electronic ground state. In Table 5 the vibrational frequencies of the CO stretch vibration extracted from our photoelectron data are listed. All values exhibit a considerable uncertainty, which is caused by the relatively large peak width of the single vibrational transitions. In addition, in some cases the peaks are asymmetric indicating the superposition of an unresolved fine structure due to the excitation of low energy vibrational modes. Our data can be directly compared with IR and HREELS data of surface adsorbed molecules and carbonyls (Tables 1 and 2). In photoelectron spectroscopy the symmetric mode is excited only.

The measured C–O stretch vibration frequency of $Ni_1(CO)_3^-$ ($2090 \pm 80\ cm^{-1}$; Table 5) agrees with the one of the earlier experiment from Stevens et al. [87] ($2100 \pm 80\ cm^{-1}$). These values can be directly compared with IR data of the neutral species measured in an argon matrix (Table 2: $2120\ cm^{-1}$). The frequency is slightly larger than the one of CO adsorbed to a Ni surface (Table 1: $2045–2069\ cm^{-1}$). The frequencies found for the saturated $Ni_n(CO)_m^-$ and $Pt_n(CO)_m^-$ species are all in between $2020–2120\ cm^{-1}$ (Table 5) and therefore are similar to the ones of CO molecules adsorbed on-top on a metal surface (Table 1). This supports the general idea that the similarity of the frequencies of carbonyls and CO molecules adsorbed on surfaces indicates a corresponding similarity of the strength of the chemisorption bond.

Table 5
CO stretch frequencies extracted from photoelectron spectra

$Ni_1(CO)_3^-$	2090 ± 80
$Ni_2(CO)_1^-$	1800 ± 80
$Ni_2(CO)_4^-$	2040 ± 80
$Ni_3(CO)_1^-$	1750 ± 80
$Ni_3(CO)_4^-$	2090 ± 100
$Ni_3(CO)_6^-$	2040 ± 80
$Pd_2(CO)_2^-$	2040 ± 80
$Pd_3(CO)_2^-$	1950 ± 80
$Pt_1(CO)_3^-$	2060 ± 80
$Pt_2(CO)_5^-$	2120 ± 80
$Pt_3(CO)_6^-$	2020 ± 60
$Pt_4(CO)_8^-$	2050 ± 150

Vibrational frequencies of the C–O stretch mode of the neutral electronic ground state as extracted from the photoelectron spectra. All values are given in wavenumbers (cm^{-1}).

This similarity is also supported by the experiment from Longoni et al. [47], who found a on-top frequency of $2065\ cm^{-1}$ and a bridge frequency of $1875\ cm^{-1}$ for $(Pt_3(CO)_6)_6^{2-}$ carbonyl cluster ions in solution. $Pt_3(CO)_6^{2-}$ is planar with a triangular metal core and three COs bound on-top to each metal atom and three COs bound in bridge sites connecting two metal atoms. The value of $2065\ cm^{-1}$ corresponds roughly to our measurement of the CO stretch frequency of gas phase neutral $Pt_3(CO)_6$ (Table 5). It is interesting, that in our experiment only the on-top frequency is observed. The 12 2π orbitals of the 6 CO ligands form 12 molecular orbitals, of which the one with the highest stability is occupied by the additional electron of the anion. Our observation indicates, that only the 2π orbitals of on-top bound COs contribute to this orbital.

$Ni_2(CO)_1^-$ and $Ni_3(CO)_1^-$ exhibit extremely lowCO stretch frequencies (Table 5). The

frequencies are much lower than the ones of the saturated clusters for two reasons: (i) the single CO molecule is most likely bound in either a bridge or a hollow site and (ii) the CO stretch frequency decreases with decreasing number of ligands (Table 2, [43]). Grushow et al. [96] found an enhanced binding energy of the first three CO molecules bound to a Pt_3^- cluster (Table 3). The similarity of the three binding energies indicates similar adsorption sites, which are probably the three bridge sites of the triangular Pt_3 core. We found a general similarity of the photoelectron spectra of the saturated $Ni_n(CO)_m^-$ and $Pt_n(CO)_m^-$ clusters, which is supported by the similar geometric [48] and electronic [60] structures of $Ni_3(CO)_6^{2-}$ and $Pt_3(CO)_6^{2-}$.

The C–O stretch vibrations found for the $Ni_n(CO)_1^-$ species are lower than any such frequencies measured for CO adsorbed on a Ni surface [102]. This is in analogy to the measured binding energy of CO to a Pt_3^- cluster, which is about twice the value of the corresponding surface. The low C–O stretch frequencies indicate an increased π-backdonation to be responsible for the increased binding energy found for $Pt_3(CO)_1^-$. The π-backdonation contribution to the chemisorption bond is stronger for bridge bonded ligands than for the ones bound in on-top sites, which explains the normal binding energy of the on-top ligands of $Pt_3(CO)_m^-$. The observation that the π-backdonation is stronger for small clusters might be a key to the understanding of the catalytic properties of small particles.

The energy resolution of the spectrometer depends on the kinetic energy of the electrons. If the photon energy is adjusted to be slightly above the emission threshold, the electrons corresponding to the transition into the neutral electronic ground state are slow and vibrational fine structure can be resolved in more detail. Fig. 17 displays such a high resolution spectrum of $Pt_3(CO)_6^-$. Apart from the CO stretch vibration (A, B) a second progression corresponding to the excitation of a low energy vibration mode (A, D, E; 425 ± 30 cm^{-1}) is observed. This frequency is similar to the one of the vibration of a CO molecule versus a Pt surface [103] and can therefore be assigned to the vibration of the CO molecules versus the metal core of the carbonyl. A similar mode has been found for the transition into the first excited state of neutral $Ni_1(CO)_3^-$ (see above). The observation of such a vibrational mode indicates, that the chemisorption bond length is altered owing to the emission process. This is to be expected for photodetachment from the antibonding 2π hybrid orbital corresponding to the appearance of the 2π peak in the spectra. Probably, a similar low energy mode is superimposed on all the progressions assigned to the C–O stretch vibration. This explains the broad peaks of the individual vibrational transitions and, in some cases, the asymmetric shape responsible for the large error of the values listed in Table 5.

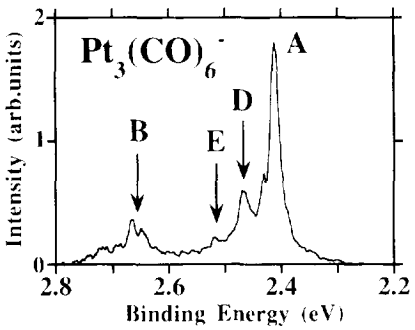

Fig. 17. High resolution photoelectron spectrum of $Pt_3(CO)_6^-$ recorded with a photon energy of $h\nu$ = 3.0 eV. The peaks marked A, B correspond to the ones in Fig. 7.

5. Conclusions

Our observations can be summarized in the following main points:

1. The appearance of the characteristic 2π peak in the spectra of the saturated $Pt_n(CO)_m^-$ species indicates, that saturation is caused by the formation of an electronic closed shell (Fig. 1). As predicted by theory, the average configuration of a Pt atom changes from d^9s to d^{10}

(Fig. 2). This agrees with the general idea of the electron counting rules, but the large differences in the electronic structure of the isoelectronic $Ni_n(CO)_m^-$, $Pd_n(CO)_m^-$ and $Pt_n(CO)_m^-$ species mirrored in the photoelectron spectra demonstrates the danger in the use of this oversimplified picture. Consequently, differences in the saturation limits might be due to electronic effects and not, as predicted by the counting rules, owing to differences in the geometries of the metal cores. Saturation in clusters is different from the formation of a monolayer on a metal surface, which is limited by steric effects.

2. The Blyholder model for chemisorption (Figs 1 and 2) explains several of our observations like the appearance of the characteristic 2π peak and its vibrational fine structure and the similarity of the spectra of the saturated $Ni_n(CO)_m^-$ and $Pt_n(CO)_m^-$ clusters. This general picture is supported by high level calculations of the electronic structure of $Ni_3(CO)_6^-$ and $Pt_3(CO)_6^-$ [60].
3. The 2π peak in the spectrum of $Ni_1(CO)_1^-$ [87] has been assigned to emission from a metal s derived orbital [68]. This seems to be in disagreement with the general assignment of the 2π peaks in our spectra to emission from a CO 2π-derived orbital. However, according to Fig. 2 the destabilization of the metal s–orbital increases with an increasing amount of CO ligands. In $Ni_1(CO)_1^-$ this orbital might be still more stable than the CO 2π orbitals. In $Ni_1(CO)_2^-$ the level ordering can be reversed with one of the CO 2π-derived orbitals being more stable than the further destabilized metal s orbital. This picture is supported by the change in the Frank–Condon profile of the 2π peaks. In $Ni_1(CO)_1^-$ the intensity of the $1 \leftarrow 0$ vibrational transition of the 2π peak is weaker with respect to the $0 \leftarrow 0$ feature than in the spectra of $Ni_1(CO)_2^-$ and $Ni_1(CO)_3^-$. This indicates, that the admixture of CO 2π character to the corresponding orbital is smaller (but not zero) for $Ni_1(CO)_1^-$ then for $Ni_1(CO)_2^-$ and $Ni_1(CO)_3^-$.
4. The observation of the antibonding $(d_{z^2}-5\sigma)$ hybrid orbital in the spectrum of $Ni_1(CO)_3^-$ is new and based upon the observation of the vibrational fine structure. The position of the $(d_{z^2}-5\sigma)$ hybrid orbital at the upper edge of the occupied metal d band agrees with several theoretical predictions. It also supports the prediction from Bagus et al. [66], who found a non-bonding contribution from the $5\sigma/d_{z^2}$ interaction for Ni, because the antibonding orbital is occupied.
5. The 2π peak found in many of our PES is assigned to the emission from the most stable CO 2π-derived orbital, which is the LUMO in case of the saturated neutral clusters. The HOMO–LUMO gap can be estimated from the spectra and it is found to decrease strongly with the increasing number of metal atoms (estimates from Figs 7, and 10: $Pt_1(CO)_3^- \approx$ 2.5 eV; $Pt_3(CO)_6^- < 0.5$ eV). On surfaces, the position of the lower edge of the CO 2π band is located about 1.5 eV above the Fermi energy [6–9]. For example, in the carbonyls the lowest 2π-derived orbitals are more stable than on a surface. This is synonymous with the increased π-backdonation in clusters and/or a stronger mixing with unoccupied metal p orbitals induced by the lower symmetry compared with a surface.
6. The CO stretch vibration frequency found for several saturated species agrees roughly with the corresponding surface data. Previously this has been taken as evidence for the assumed similarity of the chemisorption bond of CO to a metal surface and in a carbonyl. However, for the stretch frequencies of clusters with a single CO ligand we find an extremely low frequency. This demonstrates the importance of measurements of species with a low coverage, since for both clusters and surfaces the stretch frequencies depend on the CO coverage. The low frequencies indicate a stronger π-backdonation in agreement

with a recent measurement of the binding energy of a single CO molecule to a Pt_3^- cluster [96]. A stronger π-backdonation might be one key information to understand the catalytic properties of small transition metal clusters. Furthermore, if this observation is a general difference between small particles and surfaces, it might explain some of the difficulties to describe surface data by cluster calculations using a small number of metal atoms only.

7.

In contrast to Pt the PES of the unsaturated $Ni_n(CO)_m^-$ clusters exhibit a 2π peak indicating the occupation of a 2π-derived orbital by the additional electron. The neutral species are expected to have unoccupied metal d-derived orbitals with a higher stability than the 2π-derived orbitals. The preference of the additional charge to occupy the more delocalized 2π orbital is explained by the relatively high Coulomb repulsion in the Ni 3d orbitals. If the additional electron occupies one of the localized Ni 3d orbitals this would correspond to a change in configuration from $(d^9)^n 2\pi$ to $(d^9)^{n-1}d^{10}$ (the notation $(d^9)^n$ indicates the highly localized $3d^9$ orbitals of the n Ni atoms in the cluster), which costs in the bare Ni atom an additional energy of about 1.7 eV ($d^9s \rightarrow d^{10}$). Such correlation effects also show up in the spectra of the bare clusters, which are related to the ferromagnetic properties of small Ni_n^- clusters [98].

8.

The spectra of the saturated and unsaturated Pd species show no pronounced features except the ones of the $Pd_n(CO)_2^-$ clusters. These exhibit a 2π peak like the spectra of the saturated Ni and Pt clusters. This might indicate a partial saturation and a possible higher stability of the species with two ligands. It would be interesting to compare the photoelectron spectra to measurements of the ligand binding energies similar to the ones conducted for $Pt_3(CO)_m^-$ [96].

9.

In small Pd clusters the atoms have a configuration closer to d^{10} caused by the higher relative stability of the Pd 4d orbitals compared with the Ni and Pt 3d and 5d orbitals. With increasing cluster size the Pd 5s and 4d bands broaden and the Pd atom configurations approach d^9s similar to Ni and Pt ($d^{8.6}s^{1.4}$, $d^{8.7}s^{1.3}$ and $d^{8.2}s^{1.8}$ for bulk Ni, Pd and Pt, respectively [94]). This explains the similarity of the CO bond for the three metal surfaces. A d^{10} configuration corresponds to an electronic closed shell with a lower polarizability, i.e. a lower ability to form a bond with the ligand orbitals. Both bonding mechanisms, σ-donation and π-backdonation, are expected to be weaker. This might explain the known instability of Pd carbonyls. However, the saturation limits determined in the gas phase experiments are approximately similar ($\pm$ 1 ligand) for the three metals.

We demonstrated the power of vibrationally resolved photoelectron spectroscopy of mass-separated cluster anions to study chemisorption of CO on transition metal particles. The high resolution allows in some cases the determination of the CO stretch frequency and the frequency of the metal–CO vibration mode. The electronic information corresponding to the main features observed in the spectra in combination with the vibrational information corresponding to the fine structure of single features allow a detailed analysis of the electronic interactions which form the chemisorption bond. This type of spectroscopy might be very useful to understand the wealth of data on the reactivities and saturation limits of clusters determined in reaction type experiments and the differences in the catalytic activities of small particles.

References

[1] R. Hoffmann, Rev. Mod. Phys., 60 (1988) 601.
[2] G. Blyholder, J. Phys. Chem., 68 (1964) 2772.
[3] H.J. Freund and H. Kuhlenbeck, Band-structure determination of adsorbates. In: W. Eberhardt (Ed.), Applications of Synchrotron Radiation, Springer Series in Surface Science, Vol. 35 Springer, Berlin, 1994, p. 9.

[4] J.C. Campuzano, The adsorption of carbon monoxide by the transition metals. In: D.A. King (Ed.), Chemistry and Physics of Solid Surface Heterogeneous Catalysts, Vol. 3A, Elsevier, Amsterdam, 1990, p. 389.
[5] G. Ertl, J. Küppers, Low Energy Electrons and Surface Chemistry, VCH, Weinheim, 1985.
[6] J. Rogozik and V. Dose, Surf. Sci., 176 (1986) L847.
[7] P.D. Johnson and S.L. Hulbert, Phys. Rev. B, 35 (1987) 9427.
[8] K.H. Frank, H.-J. Sagner, E.E. Koch and W. Eberhardt, Phys. Rev. B, 38 (1988) 8501.
[9] N. Memmel, G. Rangelow, E. Bertel, V. Dose, K. Kometer and N. Rösch, Phys. Rev. Lett., 63 (1989) 1884.
[10] F.M. Hoffman, Infrared reflection–absorption spectroscopy of adsorbed molecules, Surf. Sci. Rep., 3 (1983) 107–192.
[11] R. Caudano, J.-M. Gilles and A.A. Lucas (Eds.), Vibrations at Surfaces, Plenum, New York, 1982.
[12] D. Hoge, M. Tüshaus, E. Schweizer, A.M. Bradshaw, Chem. Phys. Lett., 151 (1988) 230.
[13] H. Steiniger, S. Lehwald, H. Ibach, Surf. Sci., 123 (1982) 264.
[14] S. Andersson, Solid State Commun., 21 (1977) 75.
[15] B.N.J. Persson and R. Ryberg, Phys. Rev. B, 24 (1981) 6954.
[16] B.E. Hayden and A.M. Bradshaw, Surf. Sci., 125 (1983) 787.
[17] P.S. Bagus, C.J. Nelin and C.W. Bauschlicher, Jr., Phys. Rev. B, 28 (1983) 5423.
[18] N.V. Richardson and A.M. Bradshaw, Surf. Sci., 88 (1979) 255.
[19] J.N. Allison, W.A. Goddard III, Surf. Sci., 115 (1982) 553, and references cited therein.
[20] J.N. Allison, W.A. Goddard III, Surf. Sci., 110 (1981) L615.
[21] H. Jörg, N. Rösch, Surf. Sci., 163 (1985) L627, and references cited therein.
[22] W. Müller and P.S. Bagus, J. Vac. Sci. Technol. A, 3 (1985) 1623.
[23] P.S. Bagus, C.J. Nelin and C.W. Bauschlicher, Jr., J. Vac. Sci. Technol. A, 2 (1984) 905.
[24] F. Raatz and D.R. Salahub, Surf. Sci., 176 (1986) 219.
[25] G.F. Holland, D.E. Ellis and W.C. Trogler, J. Chem. Phys., 83 (1985) 3507.
[26] C.W. Bauschlicher, Jr., and C.J. Nelin, Chem. Phys., 108 (1986) 275.
[27] G. Pacchioni and P.S. Bagus, J. Chem. Phys., 93 (1990) 1209.
[28] A. Goursot, I. Papai and D.R. Salahub, J. Am. Chem. Soc., 114 (1992) 7452.
[29] G. Pacchioni and J. Koutecky, J. Phys. Chem., 91 (1987) 2658.
[30] A. Gavezotti, G.F. Tantardini and H. Miessner, J. Phys. Chem., 92 (1988) 872.
[31] N.K. Ray and A.B. Anderson, Surf. Sci., 119 (1982) 35.
[32] P. Shiller and A.B. Anderson, Surf. Sci., 236 (1990) 225.
[33] D. Drakova and G. Doyen, Surf. Sci., 226 (1990) 263.
[34] Yat-Ting Wong and R. Hoffmann, J. Phys. Chem., 95 (1991) 859, and references cited therein.
[35] Shen-Shu Sung and R. Hoffmann, J. Am. Chem. Soc., 107 (1985) 578.
[36] E. Wimmer, C.L. Fu and A.J. Freeman, Phys. Rev. Lett., 55 (1985) 2618.
[37] A.H. Cowley, U.V. photoelectron spectroscopy in transition metal chemistry. In S.J. Lippard (Ed.), Progress in Inorganic Chemistry, Vol. 26, Wiley, New York, 1979, and references cited therein.
[38] E.W. Plummer, W.R. Salaneck and J.S. Miller, Phys. Rev., 18 (1978) 1673.
[39] H.-J. Freund and E.W. Plummer, Phys. Rev. B, 23 (1981) 4859.
[40] P.S. Braterman, Metal Carbonyl Spectra, Academic Press, London, 1975.
[41] R.L. DeKock, Inorg. Chem., 10 (1971) 1205.
[42] C. de la Cruz and N. Sheppard, J. Mol. Struct., 224 (1990) 141.
[43] J.A. Timney, Inorg. Chem., 18 (1979) 2502.
[44] E.P. Kündig, D. McIntosh, M. Moskovits and G.A. Ozin, J. Am. Chem. Soc., 95 (1973) 7234.
[45] F.A. Cotton and C.S. Kraihanzel, J. Am. Chem. Soc., 84 (1962) 4432.
[46] J.C. Calabrese, L.F. Dahl, A. Cavalieri, P. Chini, G. Longoni and S. Martinengo, J. Am. Chem. Soc., 96 (1974) 2614.
[47] G. Longoni and P. Chini, J. Am. Chem. Soc., 98 (1976) 7225.
[48] J.C. Calabrese, L.F. Dahl, P. Chini, G. Longoni and S. Martinengo, J. Am. Chem. Soc., 96 (1974) 2616.
[49] A. Misono, Y. Uchida, M. Hidai and K. Kudo, J. Organometal. Chem., 20 (1969) P7.
[50] D.J. Underwood, R. Hoffmann, K. Tatsumi, A. Nakamura and Y. Yamamoto, J. Am. Chem. Soc., 107 (1985) 5968.
[51] D.G. Evans, J. Organometal. Chem., 352 (1988) 397.
[52] See, e.g., a recent review: G. Schmidt (Ed.), Cluster and Colloids, VCH, Weinheim, 1994.
[53] G. Pacchioni, L. Ackermann and N. Rösch, Gazz. Chim. Italiana, 122 (1992) 205.
[54] D.A. van Leeuwen, J.M. van Ruitenbeek, L.J. de Jongh, A. Ceriotti, G. Pacchioni, O.D. Häberlen and N. Rösch, Phys. Rev. Lett., 73 (1994) 1432.
[55] N. Rösch, L. Ackermann and G. Pacchioni, J. Am. Chem. Soc., 114 (1992) 3549.
[56] N. Rösch, L. Ackermann and G. Pacchioni, Inorg. Chem., 32 (1992) 2963.
[57] C.W. Bauschlicher, Jr., and P.S. Bagus, J. Chem. Phys., 81 (1984) 5889.
[58] R.G. Woolley, Chem. Phys. Lett., 143 (1988) 145.
[59] D.W. Bullett, Chem. Phys. Lett., 135 (1987) 373.
[60] D.W. Bullett, Chem. Phys. Lett., 115 (1985) 450.
[61] M.R.A. Blomberg, P.E.M. Siegbahn, T.J. Lee, A.P. Rendell and J.E. Rice, J. Chem. Phys., 95 (1991) 5898.
[62] J.W. Lauher, J. Am. Chem. Soc., 100 (1978) 5305.
[63] J.W. Lauher, J. Am. Chem. Soc., 101 (1979) 2604.
[64] S.M. Owen, Electron counting in clusters: A view of the concept, Polyhedron Rep. 23. In: Polyhedron, 7 (1988) 253.
[65] A.B. Rives and R.F. Fenske, J. Chem. Phys., 75 (1981) 1293.
[66] C.W. Bauschlicher, Jr., P.S. Bagus, C.J. Nelin and B.O. Roos, J. Chem. Phys., 85 (1986) 354.
[67] M. Blomberg, U. Brandemark, J. Johansson, P. Siegbahn and J. Wennerberg, J. Chem. Phys., 88 (1988) 4324.
[68] C.W. Bauschlicher, Jr., L.A. Barnes and S.L. Langhoff, Chem. Phys. Lett., 151 (1988) 391.
[69] G.W. Smith and E.A. Carter, J. Phys. Chem., 95 (1991) 2327.

[70] C.M. Rohlfing and P.J. Hay, J. Chem. Phys., 83 (1985) 4641.
[71] I. Papai, A. Goursot, A. St-Amant and D.R. Salahub, Theor. Chim. Acta, 84 (1992) 217, and references cited therein.
[72] M.R.A. Blomberg, C.B. Lebrilla and P.E.M. Siegbahn, Chem. Phys. Lett., 150 (1988) 522.
[73] S. Roszak and K. Balasubramanian, J. Phys. Chem., 97 (1993) 11238.
[74] H. Basch, Chem. Phys. Lett., 116 (1985) 58, and references cited therein.
[75] W. de Heer, Rev. Mod. Phys., 65 (1993) 611.
[76] N. Rösch and G. Pacchioni. In G. Schmidt (Ed.), Clusters and Colloids, Verlag Chemie, Weinheim, 1994, p.5.
[77] P. Fayet, M.J. McGlinchey and L.H. Wöste, J. Am. Chem. Soc., 109 (1987) 1733.
[78] D.M. Cox, K.C. Reichmann, D.J. Trevor and A. Kaldor, J. Chem. Phys., 88 (1987) 111.
[79] B.C. Guo, K.P. Kerns and A.W. Castleman, Jr., J. Chem. Phys., 96 (1992) 8177.
[80] Xiaoli Ren, P.A. Hintz and K.M. Ervin, J. Chem. Phys., 99 (1993) 3575.
[81] P.A. Hintz and K.M. Ervin, J. Chem. Phys., 100 (1994) 5715.
[82] E.K. Parks, L. Zhu, J. Ho and S.J. Riley, J. Chem. Phys., 100 (1994) 7206.
[83] P.A. Hintz and K.M. Ervin, J. Chem. Phys., 103 (1995) 7897.
[84] O. Cheshnovsky, S.H. Yang, P.L. Pettiette, M.J. Craycraft and R.E. Smalley, Rev. Sci. Instrum., 58 (1987) 2131.
[85] C.Y. Cha, G. Ganteför and W. Eberhardt, Rev. Sci. Instrum., 63 (1992) 5661.
[86] H. Handschuh, G. Ganteför and W. Eberhardt, Rev. Sci. Instrum., 66 (1995) 3838.
[87] A.E. Stevens, C.S. Feigerle and W.C. Lineberger, J. Am. Chem. Soc., 104 (1982) 5026.
[88] A. Nakajima, T. Taguwa and K. Kaya, Chem. Phys. Lett., 221 (1994) 436.
[89] A.A. Bengali, S.M. Casey, C. Cheng, J.P. Dick, P.T. Fenn, P.W. Villalta and D.G. Leopold, J. Am. Chem. Soc., 114 (1992) 5257.
[90] G. Herzberg, Molecular Spectra and Molecular Structure, Vol. II, Van Nostrand, New York, 1945.
[91] R.G. Tobin, R.B. Phelps and P.L. Richards, Surf. Sci., 183 (1987) 427.
[92] M.E. Davila et al., Surf. Sci., 311 (1994) 337.
[93] J. Ho, M.L. Polak, K.M. Ervin and W.C. Lineberger, J. Chem. Phys., 99 (1993) 8542.
[94] S. Blügel, personal communication (1996).
[95] L.S. Sunderlin, Dingneng Wang and R.R. Squires, J. Am. Chem. Soc., 114 (1992) 2788.
[96] A. Grushow and K.M. Ervin, J. Am. Chem. Soc., 117 (1995) 11612.
[97] See, e.g., J.E. Huheey, Inorganic Chemistry, Harper and Row, New York, 1983.
[98] G. Ganteför and W. Eberhardt, Phys. Rev. Lett., 76 (1996) 4975.
[99] K.M. Ervin, J. Ho and W.C. Lineberger, J. Chem. Phys., 89 (1988) 4514.
[100] J. Ho, K.M. Ervin, M.L. Polak, M.K. Gilles and W.C. Lineberger, J. Chem. Phys., 95 (1991) 4858.
[101] J.J. Yeh and I. Lindau, Atomic Data and Nuclear Data Tables, 32 (1985) 1.
[102] L. Surnev, Z. Xu and J.T. Yates, Jr., Surf. Sci., 201 (1988) 1.
[103] W.D. Mieher, L.J. Whitman and W. Ho, J. Chem. Phys., 91 (1989) 3228.